NTNU
Norwegian University of
Science and Technology

Removal of Aluminium Carbide from Liquid Aluminium

Trygve Storm Aarnæs

Materials Science and Engineering (MTMT)
Submission date: June 2018
Supervisor: Gabriella Tranell, IMA

Norwegian University of Science and Technology
Department of Materials Science and Engineering

1 Preface

The following thesis is the result of a five year master programme at The Norwegian University of Science and Technology, at Department of Materials Science and Engineering. My project was funded by Best, the work accounts for 30 ECTS, where most of the project was performed during the two semesters of fall 2017 and spring 2018.

I wish to thank my supervisor Professor Gabriella Tranell for constructive guidance through my specialisation project and my masters work. I would also like to thank Mertol Gökelma for the time he spent helping me with the writing process, and discussing aspects of experimental work and the results that were obtained.

Furthermore, I would also like to thank Ivar Andre Ødegård for helping me, sometimes on very short notice, with building my setup, Jurgen Maier from the Institute IME Process Metallurgy and Metal Recycling, RWTH Aachen University for helping me through the experimental work in my specialisation project, and Svend Grådahl for finding me a humidity sensor on short notice, last but not least I wish to thank Heiko Gaertner who operated the FTIR for working around a very tight lab schedule.

2 Abstract

Aluminium carbide (Al_4C_3) inclusions are a common type of impurity found in aluminium alloys. Currently aluminium carbide cannot be efficiently removed due to its small particle size and wetting properties. The small carbide inclusions can lead to surface defects, in addition some products have a very low tolerance for carbide content.

In this project it was attempted to remove carbide inclusions from aluminium, which was sampled from an electrolysis cell. Preliminary experiments indicated H_2O in argon to be a promising candidate for a gas based removal strategy. [1] Experiments were performed in a lab-scaled furnace, with gas mixes with 1% and 2% H_2O in argon. Additional experiments to examine the effect of remelting aluminium at 700°C, 750°C and 800°C were performed. The carbide content of the metal was examined before, right after melting and after each experiment, dross samples were also analysed. The off-gas was analysed by an FTIR-spectrometer.

Secondary experiments aimed towards examining the formation of carbide was also performed. Carbide was formed by heating pure aluminium to 1100°C in a graphite crucible. Afterwards the samples were examined in SEM.

A setup was built which is capable of performing gas injection into molten aluminium. In the off-gas methane was detected, which is evidence of chemical removal of carbide. The remelting experiments gave a reduction in carbide content which increases with temperature. Metallographic analysis found appearance and size of the carbide inclusions to be in line with previous observations. [2]

This thesis first attempts to gain an overview of existing research relating to the removal of Al_4C_3. Then results are presented concerning the carbide removal ability of the different reactive gases, as well as the off-gas compositions. Lastly different mechanisms explaining the observed behaviour is proposed.

3 Sammendrag

Aluminiumkarbid (Al_4C_3) partikler er en vanlig type urenhet som finnes i aluminiumslegeringer. Nå for tiden er det ikke mulig å fjerne aluminiumkarbid på en effektiv måte på grunn av en liten partikkelstørrelse og dårlige fuktningsegenskaper. Karbidpartikler som ender opp i sluttproduktet kan føre til overflatedefekter, i tillegg har enkelte produkter ekstremt trange toleranser for karbidinnhold.

I dette prosjektet ble det forsøkt å fjerne aluminiumkarbid fra aluminium som ble tatt fra en elektrolysecelle. Tidligere eksperimenter indikerte at H_2O i argon er en lovende kandidat for en gassbasert raffineringsstrategi. [1] Eksperimentene ble utført i en lab-skala ovn, med gassblandinger med 1% eller 2% H_2O i argon. Ekstra eksperimenter ble utført for å undersøke effekten av omsmeltning av aluminium ved 700°C, 750°C og 800°C. Karbidinnholdet ble målt før, like etter smeltning, og etter hvert eksperiment. Drossprøver ble også tatt. I tillegg ble avgassen analysert ved hjelp av FTIR-spektroskopi.

Det ble også utført eksperimenter med den hensikt å undersøke dannelse av karbid. Det ble dannet ved å varme opp ren aluminium til 1100°C i en grafittdigel. Etterpå ble prøvene undersøkt i SEM.

Et oppsett ble bygget som kunne blåse gass gjennom smeltet aluminium, ta prøver underveis og analysere avgassen. Metan ble detektert i avgassen noe som er en indikasjon på at den reaktive gassen reagerer med karbidet i smelten. Omsmelteforsøkene ga en reduksjon i karbidinnhold, men reduksjonen ble mindre når temperaturen ble økt. Metallografisk analyse fant karbidpartikler i samme størrelse og form som tidligere undersøkelser har rapportert. [2]

Denne avhandlingen starter med å prøve å få en oversikt over eksisterende forskning angående aluminiumkarbid. Deretter presenteres resultater angående effekten de ulike eksperimentene hadde på karbidinnholdet og avgassen. Til slutt presenteres det forslag til mekanismer som kan beskrive observasjonene som ble gjort.

Contents

4 Introduction

Aluminium alloys have become a significant part of modern society. It sees use in an incredibly wide array of applications and forms. Currently aluminium is only produced through the Hall-Heroult process from alumina dissolved in molten cryolite. During the electrolysis process, aluminium and carbon are in close physical proximity. Given the large negative change in free energy for the formation of Al_4C_3 ($\Delta G = -162\,kJ/mole$ at 700 °C [3]), it is not surprising that this compound may form. The solubility of carbon in molten aluminium decreases rapidly with temperature, so large amounts of carbide may form as the melt cools down to the lower temperatures refining operations are performed at.

This far, most of the research on Al_4C_3 has come in the form of understanding cathode wear so that the lifetime of electrolysis cells may be increased. [4] Comparatively less investigation has been done on what happens to the carbide after it leaves the electrolysis cell. Because the carbide wets the liquid metal poorly, and the size of the carbide inclusions are small, it is a real possibility that the inclusions can be transferred through all the different refining steps and end up in the finished metal.

In general inclusions are almost always harmful to the properties of the final metal. The carbide inclusions are hard and brittle, which may lead to cracks forming, which compromises the structural integrity of the product, thin products may experience formation of small pinholes. While the carbide inclusions themselves are small, the poor wetting with the aluminium lets them easily agglomerate to larger, more harmful clusters. Aluminium carbide is highly reactive and will even react with moisture present in air to form $Al(OH)_3$. The reaction leads to a volume expansion which causes ugly surface defects to form. [5]

Some products have very strict purity requirements, for example litographic sheets, and it is thus highly desirable to remove the carbide inclusions from the metal before casting.

The following project performed experiments on aluminium, sampled directly from an electrolysis cell. Preliminary experiments had already investigated various gases and found H_2O to be the most promising. [1] The main work performed was constructing an experimental setup that would allow gas injection experiments to be performed isolated from outside atmosphere, while also allowing samples to be easily taken. After the setup was built, in total 6 experiments were performed where various amounts of H_2O was added to argon which was injected into the melt. Additional experiments designed to examine the effect of remelting at 700°C,

750°C and 800°C was performed. The samples obtained through the experiments had their carbide content determined through gas chromatography which was done by Hydro Aluminium AS in Sunndalsøra.

5 Theory

The goal of this project is to examine the removal of aluminium carbide formed during the electrolysis process by utilising a reactive gas, and through just remelting. Additionally the formation of aluminium carbide will be examined. The removal process discussed in this project is intended to be performed post-tapping in a later refining step.

To achieve this, a robust understanding of how different thermodynamic and kinetic considerations affect the system is needed, as well as being aware of the current literature regarding this topic.

5.1 Process Overview of Primary Aluminium Production

Primary production of aluminium is currently done through the Hall-Héroult process. Because of alumina's high melting point of 2000°C, [3] it would pose significant material and process challenges to perform electrolysis on pure molten alumina. Instead, it is dissolved in molten cryolite (Na_3AlF_6) and the electrolysis is performed on the molten, alumina containing salt. [6]

The molten salt mix is usually referred to as the electrolyte or the bath. It contains predominantly cryolite with approximately 10-13wt% of aluminium fluoride, and around 5wt% of calcium fluoride. The maximum solubility of alumina in the bath is typically around 8wt% at the operating temperature which is approximately 960°C, but usually only 3-4wt% is added. [6] Because if too much alumina is dissolved in the bath, an undissolved alumina sludge may form and accumulate between the metal layer and the cathode block. [4] Pure cryolite has a melting point of 1013°C, [3] adding aluminium fluoride modifies the melting point to around 950°C. [6] During the operation of the cell, the bath temperature is maintained at around 5°C - 10°C above its liquidus temperature. [6]

The cell itself consists of a carbon anode that is usually a graphitised or a graphitic carbon material. The anode is immersed in the bath. Below the layer containing the bath is a layer of liquid aluminium. While the carbon block at the bottom of the cell is called the cathode block, the real electrochemical cathode is the layer of liquid aluminium. A schematic picture of the cell is displayed in figure 1. [8]

The overall reaction for the cell is as follows:

$$2\,Al_2O_3(diss) + 3\,C(s) = 4\,Al(l) + 3\,CO_2(g) \tag{1}$$

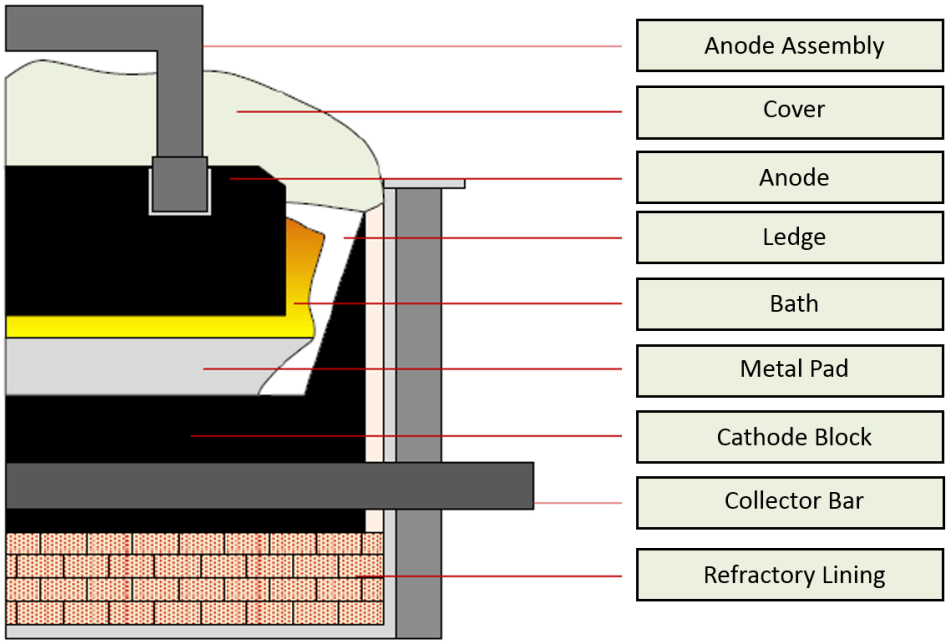

Figure 1: Illustration of an aluminium electrolysis cell. [7]

During operation of the cell, alumina is continually fed into the bath and metallic aluminium is deposited on the cathode, while $CO_2(g)$ is formed at the anode. As alumina gets reduced, the anode is consumed by the reaction and needs to be replaced at regular intervals. [4, 8]

The cathode block on the other hand, does not take part in the reaction and is just acting as an electrical connection to the cell. But despite not taking part in the reaction, it still undergoes wear. Once it has been worn down too much, the only available option is to reline the entire cell, thus the cathode wear is a major factor limiting the lifetime of the cell. [9]

After the aluminium is reduced in the electrolysis cell it still needs to go through many successive refining steps before its ready to be sold. The refinement steps themselves depend on the required composition and impurity level being produced. A general sequence of processing steps is shown in figure 2. Handling of the metal between each of the processing steps must also be done with great care, as depending on how the molten metal is handled, inclusions and impurities may be formed or transferred from one step to the next. [10] Keeping track of which chemical reactions may lead to inclusions is important, as contacting the metal with the wrong material can cause inclusions to form. [11] Thus it is not unexpected that

small inclusions such as aluminium carbide might follow the metal through all of its processing steps and end up in the final metal.

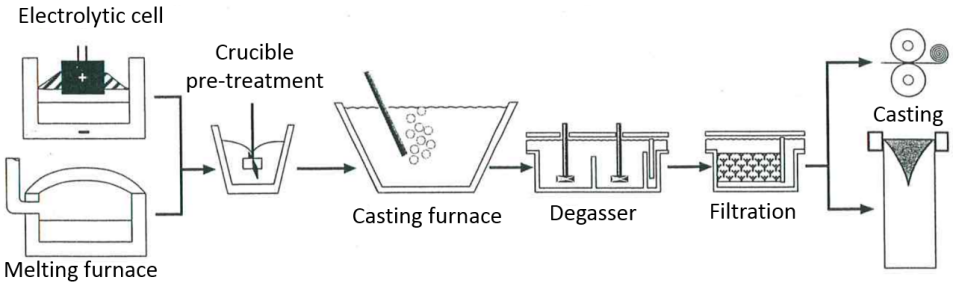

Figure 2: A sequence of molten metal processing steps. [10]

5.2 Properties and Formation Mechanisms of Al_4C_3 in Aluminium Melts

5.2.1 Carbide content

Aluminium carbide, Al_4C_3, is a very common inclusion that is found in commercially pure aluminium. [12] The particles are typically found as clusters. [5] Previous measurements of the carbide content of aluminium, taken directly from electrolysis cells performed by Simensen, reported the aluminium to contain between 50 ppm and 24 ppm of aluminium carbide, which corresponds to a carbon content of 12.5ppm to 6ppm. [13] The particles are shaped as thin discs with a diameter of 0.1µm to 5µm. [2] Furthermore, Simensen found that the carbide concentration was higher for aluminium taken from electrolysis cells being held at a higher temperature. As pointed out by Dorward, Simensen's data does not necessarily reflect the actual solubility of carbon. [14] Dorward speculated that carbon being transferred from the metal and into the bath was the reason Simensen's measurements showed a lesser concentration of carbides than equilibrium.

5.2.2 Carbide Formation

Being aware of the solubility of carbon in the melt is crucial for the understanding of the formation of Al_4C_3. Only small amounts of carbon can be dissolved in molten aluminium at temperatures used during aluminium production. Figure 3 shows the carbon aluminium phase diagram in the 600°C to 1200°C range. At 1000°C the solubility of carbon is around 40ppm, which at equilibrium corresponds to a carbide

content of 160 ppm, while it rapidly declines as the temperature approaches the melting point. [15]

There are two main mechanisms of carbide formation in a reduction cell: [5]

1. Direct reaction between liquid metal and the cathode.
2. Carbon dissolving in the metal followed by internal precipitation of carbide.

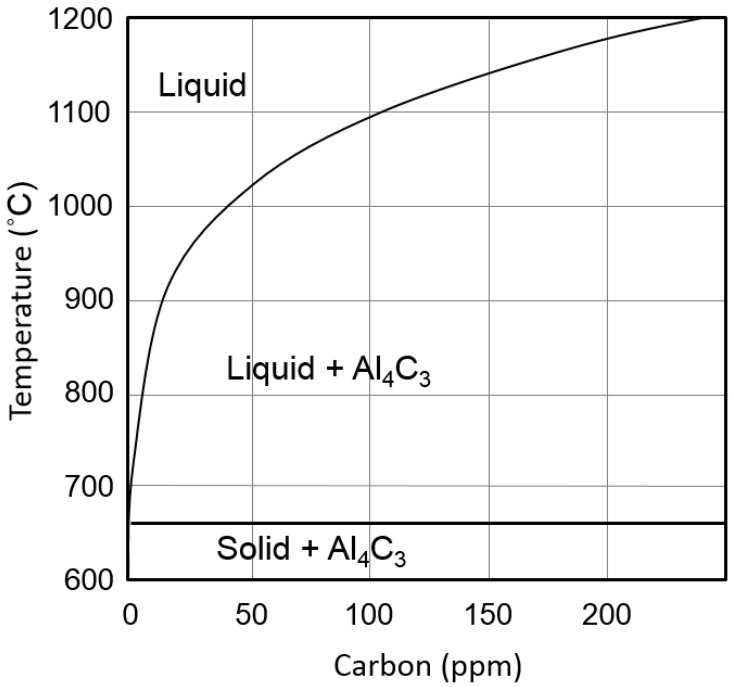

Figure 3: The aluminium carbon phase diagram. [15]

As an aluminium melt saturated with carbon is cooled slowly from 1000°C, the melt will move into the two-phase region of figure 3 where it is possible for molten aluminium to coexist with the solid aluminium carbide particles. As the melt cools down, aluminium carbide may precipitate through the direct reaction between molten aluminium and carbon: [16, 5, 17]

$$\mathrm{Al(l) + C = Al_4C_3(s)}, \quad \Delta G_{T=700^\circ C} = -162kJ \tag{2}$$

Reaction 2 has a ΔG$=-162$ kJ/mole, [3] and is thus thermodynamically favoured at typical temperatures for aluminium production. However, without

a bath present, the reaction is kinetically hindered due to a lack of direct contact between the cathode and the molten aluminium, in addition the poor wetting conditions. [18]

While it is known that carbide can form on the cathode, it may not be contributing a lot to the carbide content in the melt. Because of aluminium's poor ability to wet carbide, carbide formed through such a mechanism would have a hard time entering the melt as it would rather stick to the surface it is formed on, than let go and get mixed into the melt. [5]

The presence of cryolite can enhance the formation of carbide during production of primary aluminium. Cryolite is the molten salt electrolyte in the electrolytic production of aluminium, in which alumina is dissolved. It may be removing the protective oxide layer which provides a barrier to the direct reaction between aluminium and carbon, equation 2. It is known that liquid aluminium wets solid carbon poorly. The equilibrium wetting angle in the Al-Al_4C_3-C system was determined by Bao et al to be 126°at 700°C [19] Nonetheless, once cryolite is added, a zone forms between the carbon and the metal where perfect wetting can be achieved ($\approx 0°$); figure 4 shows a comparison of aluminium reacting with carbon, with and without cryolite present.

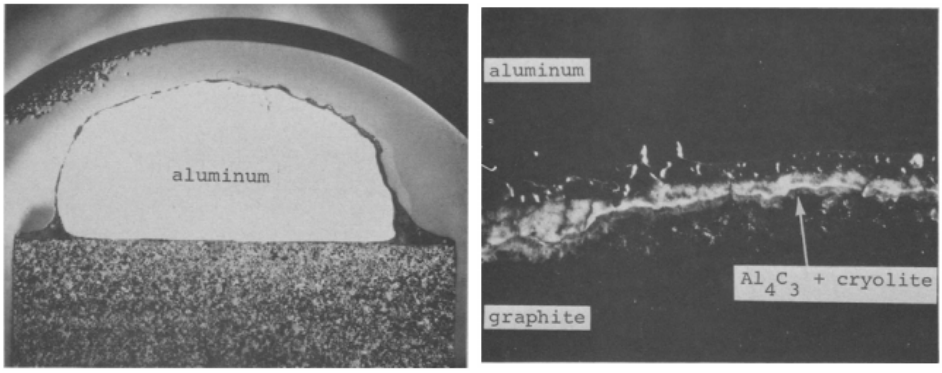

(a) With cryolite, magnification 5X. (b) No cryolite, magnification 20X.

Figure 4: Comparison of aluminium reacting with carbon with and without cryolite present. [20]

It is also worth noting that aluminium carbide is much less soluble in liquid aluminium than it is in molten cryolite, and thus by extension the bath. [9] So it may act as a solvent for the carbide formed at the C/Al interface. By removing it more is allowed to be formed. [21] The increased carbide solubility in the bath

explains why the metal is not saturated in carbon, because carbide is continuously transported from the metal and into the bath. Ødegård determined the solubility of carbide in the electrolyte to be up to 2.12wt% at 1020°C, which is 200 times more than in the metal, but varying with the molar ratio of NaF/AlF_3 as shown in figure 5. [22]

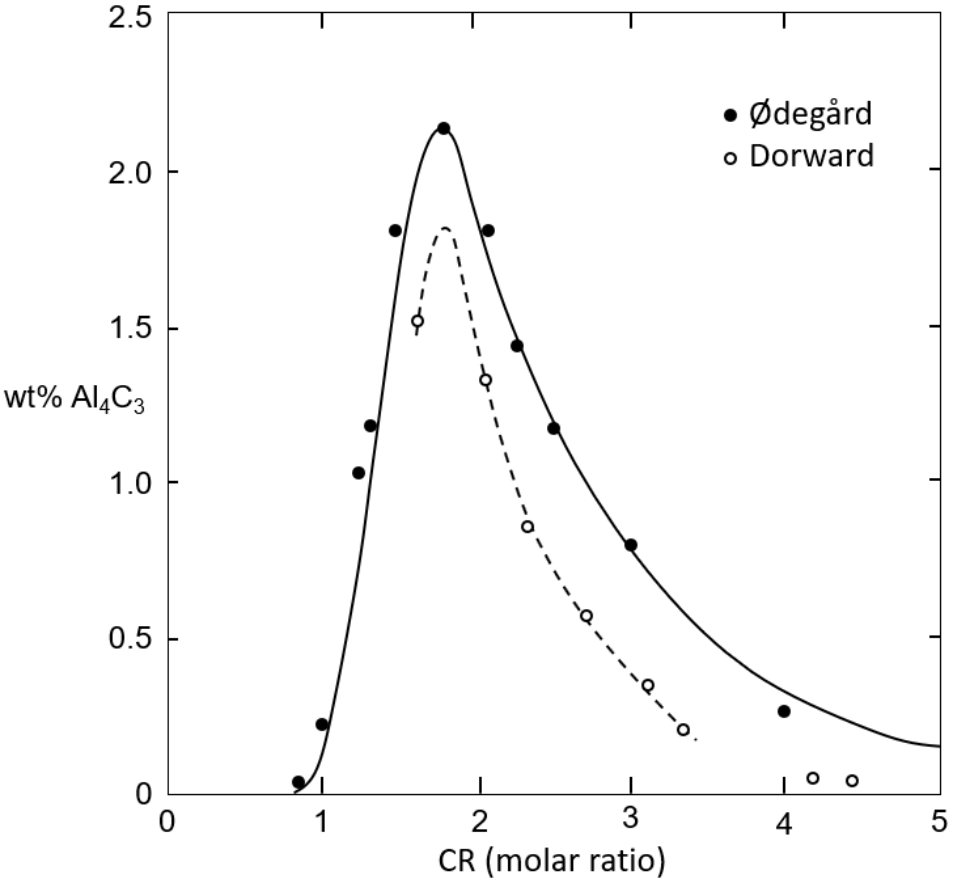

Figure 5: Solubility of Al_4C_3 in electrolyte as a function of the molar ratio of NaF/AlF_3. [22]

He found the most probable dissolution reaction for aluminium carbide dissolving in a pure NaF/AlF_3 melt to be:

$$Al_4C_3\,(s) + 5\,AlF_3(diss) + 9\,NaF\,(l) = 3\,Al_3CF_8{}^{3-} + 9\,Na^+ \qquad (3)$$

which coincides with the molar ratio of NaF/AlF_3 that yielded the maximum amount of dissolved carbide in figure 5.

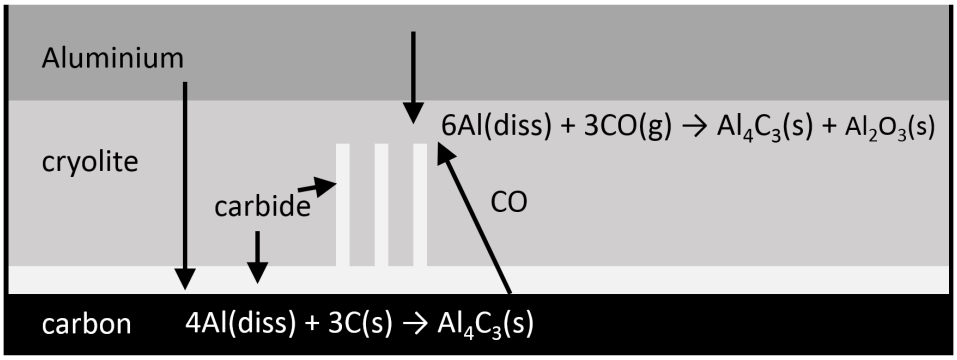

Figure 6: Proposed mechanism for aluminium carbide formation. [21]

Novak examined the influence of cryolite on the formation of aluminium carbide. [21] In diffusion couple experiments aluminium coated with a small amount of cryolite powder was cast into a graphite crucible, then a carbon pellet was placed on top. The diffusion couples were heat treated at 1030°C for times ranging from 3 hours to 3 days. At the end of the experiment the samples were quenched in water. Needles of aluminium carbide was found growing from the carbon, which was surrounded by a carbide layer. It was proposed that the cryolite helped by dissolving the protective oxide layer, and improving the wetting of aluminium on carbon. The carbide layer surrounding the carbon was suggested to form as a result of carbon diffusing through the cryolite layer, while the needles grew through a vapor-liquid-solid mechanism. When CO enters the cryolite layer, which is saturated with Al, carbide is deposited on top of the needles through reaction 4, mechanism shown in figure 6.

$$6\,\mathrm{Al} + 3\,\mathrm{CO\,(g)} = \mathrm{Al_4C_3(s)} + \mathrm{Al_2O_3(s)} \tag{4}$$

5.2.3 Size distribution of inclusions

In general there are two main ways for inclusions to grow within the melt. They may grow due to diffusion of a supersaturated component to the already formed particle. In this case carbon might may diffuse to a carbide inclusion resulting in growth. The second growth mechanism is agglomeration, two particles colliding and sticking together. [23]

First looking at growth due to carbon diffusing to the carbide inclusion. The growth rate of the inclusion is given by the total amount of carbide surface area, the supersaturation of carbon, and the mass transfer coefficient for carbon. [23]

$$\frac{dr}{dt} = \frac{k_C \rho \Delta[\%C]}{\rho_C 12 * 100} \tag{5}$$

Then the number inclusions per unit volume of melt of size r, to $r + \Delta r$, defined as $f_N(r)\Delta r$ can be determined by employing a number balance in the size interval from r to $r + \Delta r$. [23]

$$-\frac{d(V f_N(r)\Delta r)}{dt} = f_N(r)\Delta r A k_t \tag{6}$$

Here k_t is the mass transfer coefficient for the growth of carbide, and A is the surface area the carbide is removed to. The left side of equation 6 may be split into two terms. One calculating the change in size distribution function with time, and the other considers the growth of the inclusions with time. [23]

$$V\Delta r \left(\frac{\partial f_N(t,r)}{\partial t} + \frac{\partial f_N(t,r)}{\partial r} \frac{dr}{dt} \right) \tag{7}$$

If there is only a small supersaturation of carbon the second term disappears because equation 5 will equal 0. That will yield the following size distribution function: [23]

$$\frac{f_N(r,t)}{f_N(r,0)} = exp\left(-\frac{k_t A}{V} t \right) \tag{8}$$

Under stationary conditions the first term of equation 7 will disappear. This makes it possible to obtain the size distributions of inclusions in a melt that has been allowed to sit till it reaches steady state. To obtain the distribution one has to substitute equation 5 into equation 7, r_0 is a known number of inclusions of a specific size: [23]

$$\frac{f_N(r)}{f_N(r_0)} = exp\left(-\frac{(r - r_0) k_t A \rho_C 12 * 100}{\rho k_c \Delta[\%C] V} \right) \tag{9}$$

It is evident, that the size distribution of inclusions is a decreasing exponential. The particle size decreases as the ratio A/V, and k_t/k_C increases. This can be interpreted as the inclusions being removed before they are given a chance to grow into larger particles. Thus if the removal is efficient enough there will be no carbide inclusions of a large enough size affect the final product. [23]

Looking at the second growth mechanism, collisions between inclusions which then stick together. The rate of collisions is proportional to the square of concentration, [23] and as such does not usually play a major role for small concentrations, less than approximately 100ppm [23]. An exception to this rule arises because the

collision rate depends on the stirring power. [24] It is possible to generate locally very high stirring powers by employing mechanical or electromagnetic stirring, or de-gassing. [25]

The size distribution of the carbides is of importance because size plays a crucial role for the behaviour of an inclusion floating in the melt:

- As particles become smaller the effect of brownian motion grows larger leading to different movement within the melt. [26]
- Small particles have a poor filtration efficiency unless the pore size is very small, while filters with such a small pore size has very limited lifespan. [12, 27]
- Due to brownian motion dominating small particles can take a very long time to settle to the bottom of the ladle, or they may not settle at all. Same applies for flotation unless the particle attaches itself to a larger one. [28]
- During some processes such as degassing, small particles can agglomerate into larger agglomerates enhancing the removal efficiency, however the larger agglomerates are much more harmful should they remain in the metal. [26, 29]

5.2.4 Wetting Effect

The wetting properties of ceramic particles contacted by a metallic melt is of importance in several different applications. For this project the most important is for particle removal as described below.

A solid surface in contact with a liquid will have an intersection between the liquid and solid at a specific contact angle, which is also called the wetting angle. The equilibrium value of that angle can say a lot about what kind of interactions can be expected. The wetting angle is determined by the interfacial energy between the phases in contact. Figure 7 shows the wetting angle with respect to the interfacial tension γ.

If the equilibrium contact angle is less than 90° it is said that the liquid wets the solid, while for contact angles greater than 90° it is said that the solid is not wetted by the liquid, and a contact angle equal to 0 means that there is perfect wetting between liquid and the solid. [30]

Liquid aluminium is very easily oxidised, which leads to the formation of an alumina film covering the metal. Thus if for example the wetting angle between carbon and aluminium is to be examined the film must be removed. If not the

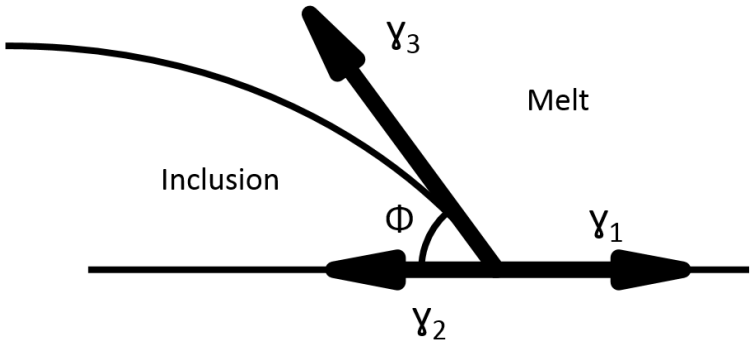

Figure 7: Interfacial tension between the different phases, and the wetting angle.

contact angle between alumina and carbon would determine what occurs, rather than the contact angle between carbon and aluminium. [30, 20]

In wetting studies of the Al/graphite system in the temperature region of 700°C to 900°C, contact angles around 100° were found, [31] furthermore the wetting angle seemed to depend strongly on temperature.

Wetting also has a strong influence on how easily a particle can nucleate. There are, broadly speaking, two types of nucleation that can occur in the aluminium melt:

1. Homogeneous nucleation.

2. Heterogeneous nucleation.

In the case of homogeneous nucleation a particle is precipitated fully surrounded by the melt. For the homogeneous nucleation of a spherical particle of radius r the change in ΔG can be expressed as follows: [32]

$$\Delta G_{hom} = -\frac{4}{3}\pi r^3 \Delta G_v + 4\pi r^2 \gamma_{SL} \tag{10}$$

Where G_v is the free energy per unit volume, and γ_{SL} is the interfacial free energy. Because the volume term of equation 10 increases with r^3 while the surface term increases with r^2, a small particle nucleating homogeneously will lead to an increase in the free energy of the melt. Thus it is possible for the melt to maintain a supersaturation of carbon without precipitating any carbide. In addition there is a critical radius, r^* that leads to a maximum increase in free energy. Any particles smaller than this are unstable and will dissolve back into the melt as that will reduce the free energy, while particles larger than $r*$ will reduce the free energy of the

melt by growing. The driving force necessary to achieve homogeneous nucleation is typically very large because of the significant contribution of the surface free energy of small particles. [23, 32]

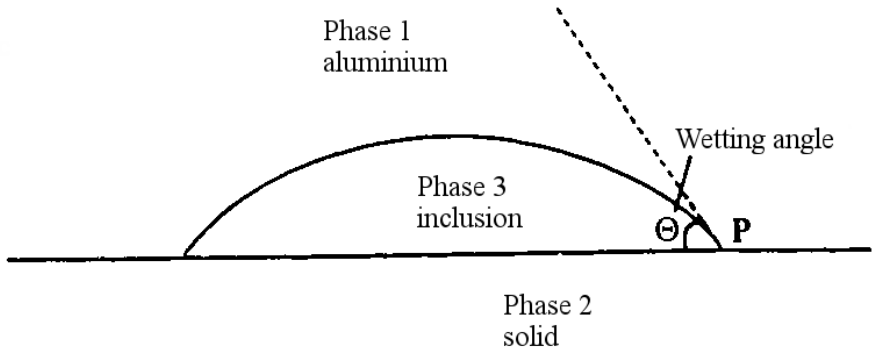

Figure 8: Heterogeneous nucleation of a solid inclusion on a solid particle. [23]

In the case of heterogeneous nucleation there are three phases involved, as in figure 8, as opposed the two phases involved for homogeneous nucleation, because a third phase is formed on the interface of the two original phases. In this case nucleation is made much easier at even small supersaturations because the interfacial energy term is reduced. The volume which minimises the energy of this system has the shape of a spherical cap with a wetting angle θ. [23]

The change in free energy as a result of heterogeneous nucleation can be written in terms of the free energy change in the homogeneous case, and a shape factor $S(\theta)$, which varies from 1 to 0 as the wetting angle changes from 0°to 180°: [32]

$$\Delta G_{het} = \Delta G_{hom} S(\theta) \tag{11}$$

It is worth noting, that as the shape factor is less or equal to 1, heterogeneous nucleation will always happen more easily than a particle forming homogeneously. For a small θ, particle formation can be catalysed on walls of a furnace or on the electrodes. As a liquid wets the new phase more efficiently, θ is reduced which lowers the barrier for nucleation. In the case of perfect wetting ($\theta = 0$) there will be no energy barrier for nucleation and it will be impossible to prevent nucleation from occurring during supersaturation. [32]

Typically homogeneous nucleation will lead to small particles distributed throughout the melt, which might occur during casting as the rapid cooling ex-

perienced as the metal is poured into the mould can create a sufficient undercooling for homogeneous nucleation to occur. Heterogeneous nucleation on the other hand favours particles forming on already existing surfaces such as already present inclusions, or the crucible walls or melt surface. [23, 32]

5.3 Possible Methods of Carbide Removal

As shielding the molten aluminium from the cathode is impossible to do, the aluminium carbide that is formed needs to be removed in a later refining operation instead. Some possible methods of removing the carbide will be presented in this section.

5.3.1 Effect of remelting

Remelting of aluminium can yield a substantial reduction in carbide content. A project performed by the author reported that by holding aluminium for 30 min at 700°C the carbide content was reduced from 39.2ppm to 3.2ppm, and at 800°C the carbide content was reduced from 39.2ppm to 7.8ppm. [1] The same effect was seen in a study performed by R. C. Dorward, [5] he attributed the effect to poor wetting between carbide and molten aluminium causing the carbide to attach itself to the crucible walls and melt surface.

5.3.2 Preliminary work/effect of various gases

In experiments carried out to compare the carbide removal efficiency of various gases. The carbide content was analysed before and after refining 1kg of aluminium with 2Nl/min of argon mixed with the reactive gas for 30 minutes. The results are displayed in figure 9.

The results indicated that moist argon shows the most promise for carbide removal, while CO_2 the worst. Furthermore it was reported that the dross collected after refining with 10% CO_2 contained orders of magnitude more carbide than the other gases used, which indicates that CO_2 might even be promoting carbide formation instead of removing it. Using 10% O_2 yielded roughly the same removal as using pure Ar and was thus assumed to not have a great effect on the carbide content. [1]

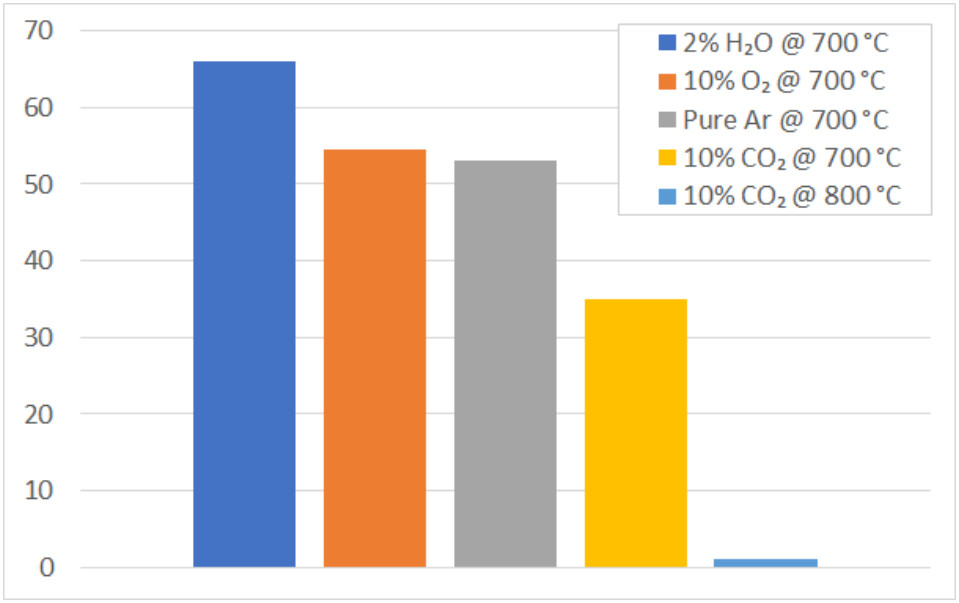

Figure 9: Removal efficiency after remelting of various gas-mixes. Results show the removal efficiency of the gas-mix divided with the removal efficiency of just remelting. [1]

5.3.3 Solid Gas Reaction

For removal reactions to occur, the reactive species must come into contact with the aluminium carbide. After the reaction has occurred, the reaction product must be removed from the melt. In the cases where the reaction product is a gas it is reasonable to assume that buoyancy forces can take care of the removal, while in the cases where alumina is formed it may leave the melt on the surface of a bubble or remain in the melt.

Some possible reactions for removing the carbide for a variety of purge gases are shown below:

$$\frac{1}{9}\,\mathrm{Al_4C_3(s)} + \mathrm{CO_2(g)} = \frac{2}{9}\,\mathrm{Al_2O_3(s)} + \frac{4}{3}\,\mathrm{CO\,(g)}, \quad \Delta G_{T=700°C} = -153.5kJ[3] \quad (12)$$

$$\frac{1}{6}\,\mathrm{Al_4C_3(s)} + \mathrm{H_2O\,(g)} = \frac{1}{3}\,\mathrm{Al_2O_3(s)} + \frac{1}{2}\,\mathrm{CH_4(g)}, \quad \Delta G_{T=700°C} = -225.8kJ[3] \quad (13)$$

$$\frac{1}{6}\,\mathrm{Al_4C_3(s)} + \mathrm{H_2O\,(g)} = \frac{1}{3}\,\mathrm{Al(OH)_3(s)} + \frac{1}{4}\,\mathrm{CH_4(g)}, \quad \Delta G_{T=700°C} = -115.3kJ[3] \quad (14)$$

$$\frac{1}{9}\,\mathrm{Al_4C_3(s)}+\mathrm{H_2O\,(g)}=\frac{2}{9}\,\mathrm{Al_2O_3(s)}+\mathrm{H_2(g)}+\frac{1}{3}\,\mathrm{CO\,(g)},\quad \Delta G_{T=700^{\circ}C}=-203.6kJ[3] \tag{15}$$

$$\frac{2}{9}\,\mathrm{Al_4C_3(s)}+\mathrm{O_2(g)}=\frac{4}{9}\,\mathrm{Al_2O_3(s)}+\frac{2}{3}\,\mathrm{CO\,(g)},\quad \Delta G_{T=700^{\circ}C}=-702.8kJ[3] \tag{16}$$

The equations show direct reactions for removing aluminium carbide inclusions, along with the ΔG for the reactions. All of the reactions have a negative Gibb's energy and are thus thermodynamically favoured to occur. [3] When using an oxygen containing gas, $\mathrm{CO\,(g)}$ is formed, which is significant as that will interact with the boudouard reaction, which will be discussed later.

Another possibility when exposing molten aluminium to $\mathrm{CO_2}$ is the following reaction: [21]

$$\frac{8}{3}\,\mathrm{Al}+\mathrm{CO_2(g)}=\mathrm{Al_4C_3}+\frac{2}{3}\,\mathrm{Al_2O_3}\quad \Delta G_{T=700^{\circ}C}=-574.6kJ[3] \tag{17}$$

If this reaction occurs, instead of removing the carbide from the melt, the $\mathrm{CO_2}$ will generate it. It has a far lower ΔG than the removal reaction associated with $\mathrm{CO_2}$, making it likely to occur instead of reaction 12. Its change in Gibb's energy increases with temperature, however not by much, at 800°C $\Delta G = -549.2$ kJ. Thus the reaction is thermodynamically favoured to happen within that temperature range. [3]

When water is added to the purge gas there are several possible reactions that may happen. Reaction 14 is the most favoured one which leaves methane as the reaction product, the other possibility is reaction 15 where $\mathrm{H_2(g)}$ is formed by the reaction. [3]

When hydrogen is formed as the reaction product it may take two possible forms. The first option is as shown in reaction 15 where it forms as $\mathrm{H_2(g)}$. The other option is that the hydrogen forms in solution in the molten aluminium, dissolving hydrogen does however require energy and would thus make the reaction less favoured thermodynamically, ΔG for hydrogen dissolution in aluminium is shown below.

$$\mathrm{H_2}=2\,\mathrm{H(diss)}\quad \Delta G_{T=700^{\circ}C}=148.8kJ[33] \tag{18}$$

The removal of the carbide particles through reactions 12, 13, 14 and 16, can be divided into four steps: [23]

1. Transport of the carbide in the melt to the vicinity of the gas bubble through a combination of diffusive and convective mass transport.

2. Transport of the carbide to the bubble/melt interface.

3. Adsorption of reactive species on the surface of the bubble.

4. Reaction between reactive species and carbide at the bubble surface.

The rate at which step 1 is happening, is controlled primarily by the degree of stirring in the melt, and the average distance the carbide particles need to be transported to reach a bubble. To make the average distance as low as possible, as many bubbles as possible should be passed through the melt. Assuming the same gas flow, smaller bubbles will yield a greater number of bubbles.

The chemical reaction is most dependent on the temperature of the system, however, at high temperatures most chemical reactions happen very rapidly.

5.3.4 Removal of dissolved carbon

In addition to the direct removal of carbide through reactions 12, 13, 14 and 16, it is also possible to remove the carbide indirectly through removing dissolved carbon from the molten aluminium. As the dissolved carbon is removed, the equilibrium displayed in equation 2 is shifted, such that the already formed carbide will dissolve back into the melt. Possible reactions are shown below in equations 19, 20 and 22:

$$\mathrm{C} + \mathrm{CO_2(g)} = 2\,\mathrm{CO\,(g)}, \quad \Delta G_{T=700^\circ C} = -82J \tag{19}$$

$$\frac{3}{2}\,\mathrm{C} + \mathrm{H_2O\,(g)} = \mathrm{CO\,(g)} + \frac{1}{2}\,\mathrm{CH_4(g)}, \quad \Delta G_{T=700^\circ C} = 4.412kJ[3] \tag{20}$$

$$\mathrm{C} + \mathrm{H_2O\,(g)} = \mathrm{CO\,(g)} + \mathrm{H_2(g)}, \quad \Delta G_{T=700^\circ C} = -50.27kJ[3] \tag{21}$$

$$2\,\mathrm{C} + \mathrm{O_2(g)} = 2\,\mathrm{CO\,(g)}, \quad \Delta G_{T=700^\circ C} = -395.9kJ[3] \tag{22}$$

Unlike the direct removal of carbide, these reactions do not all have a negative ΔG, [3] in fact the only reaction that is clearly favoured thermodynamically is 22. As can be seen from reaction 19 $\mathrm{CO_2(g)}$ is favoured over $\mathrm{CO\,(g)}$ which means that a version of the reaction forming $\mathrm{CO_2}$ instead of CO would be slightly more favoured. However, it still has a much higher ΔG than the direct carbide removing

reaction for oxygen, reaction 16. Thus, barring any kinetic considerations this carbide removal mechanism will not be preferred over the direct removal reactions.

When water is added to the purge gas there are two possible carbon removing reactions, reaction 20 forms CO(g) and CH_4(g) as the reaction product, while reaction 21 forms CO(g) and H_2(g) as the reaction product. The most thermodynamically favoured reaction is reaction 21 by a very large margin. [3] Similarly as for the solid gas reaction mechanism, it is not obvious if the hydrogen will form as H_2(g) or in solution, but the change in Gibb's energy for dissolving hydrogen in aluminium, reaction 18, causes the reaction to no longer be chemically favoured at 700°C. [33]

Reaction 19 can be recognised as the Boudouard reaction. At 700°C the metal is roughly 40°C above the melting point of aluminium where the Boudouard reaction, equation 19, is barely favoured thermodynamically. The Boudouard reaction is a highly temperature dependent reaction. It produces two moles of CO(g) per mole of CO_2(g), yielding an increase in entropy. Thus, the equilibrium constant will increase with increasing temperatures, assuming the activity of the dissolved carbon does not change much. As the equilibrium constant increases, the equilibrium composition will be favouring a lesser partial pressure of CO_2(g) and greater amount of CO(g). [3]

The change in the partial pressures of CO_2 and CO, and their temperature dependence, can be calculated from the equilibrium constant, shown below:

$$K = \frac{p_{CO}}{p_{CO_2} a_C} \tag{23}$$

Assuming constant pressure the partial pressure of CO_2 can be written as a function of the partial pressure of CO. Next the equilibrium constant is written in terms of the change in Gibb's energy.

$$K = \exp\left(-\frac{\Delta G}{RT}\right) \tag{24}$$

Combining equation 23 and 24 yields a quadratic equation that when solved, allows the partial pressures of CO and CO_2 to be expressed as a function of temperature, graphed in figure 10.

In the case of using water as the reactive gas, reaction 20, the removal reaction is not thermodynamically favoured at 700°C. But as the reaction products are gases which will quickly leave the melt due to buoyancy it may still be relevant. Also increasing the temperature reduces the change in Gibb's energy, at approximately 750°C the $\Delta G = 0$.

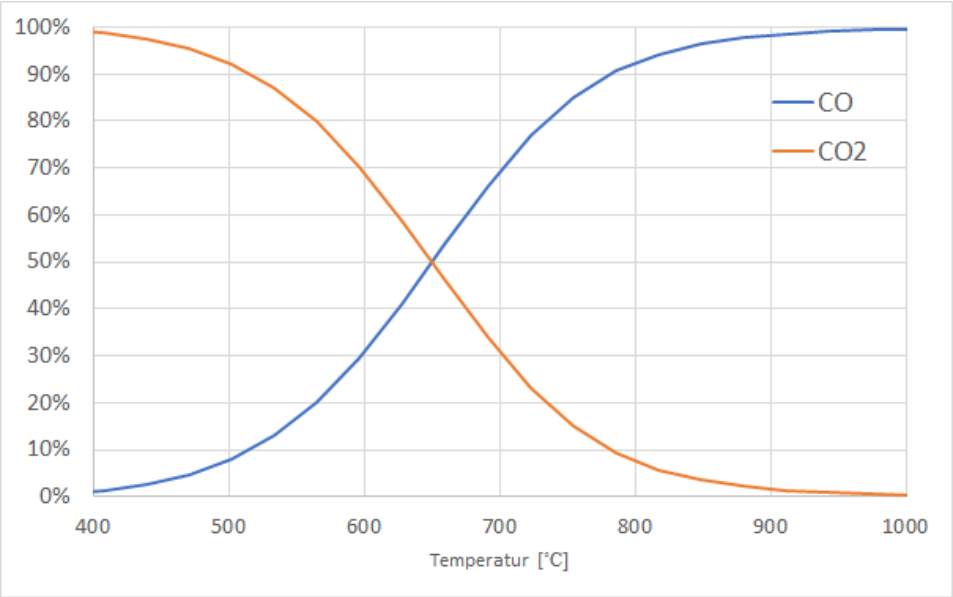

Figure 10: Temperature dependence of the Boudouard reaction.

Despite ΔG not being highly negative for reactions 19 and 20, they are not ruled out, as the final equilibrium state depends on the initial composition of the purge gas. A purge gas containing only $H_2O(g)$ or CO_2 as the reactive species will have an equilibrium state containing part $H_2O(g)$ or CO_2, and part of the reaction products.

The Boudouard reaction will also play a role in the two cases where the reactive species is H_2O or O_2 as all the other reaction forms $CO(g)$, which will be in equilibrium with carbon and CO_2.

5.3.5 Flotation

Assuming the bubble is capable of wetting the carbide inclusions, particles which come into contact with the bubbles might get stuck on the surface and traverse the melt with the bubbles until it reaches the melt surface.

To make an approximation of how many particles can be removed through this mechanism, it is assumed, that any carbide particles hitting the bubble surface are swept along. It is also important to take into account that particles are swept somewhat sideways as they approach the bubble. This effect is illustrated in figure 11 by the dotted lines showing where the inclusion will intercept the bubble.

The volume purified per second becomes the cross section of the bubble which

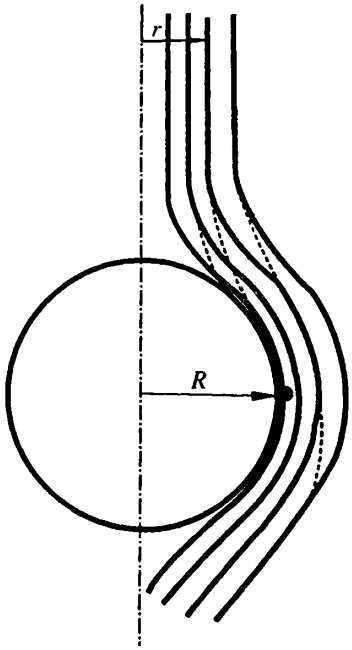

Figure 11: Collision cross-section for particles removed by a spherical particle. [23]

is multiplied with the relative velocity of the carbide inclusion and the bubble.

$$\dot{V} = \pi r^2 N v \tag{25}$$

A collision efficiency parameter, η, can be defined as the volume flow of melt with particles that will collide with the bubble divided by the total volume flow approaching the bubble. The number of particles colliding with the bubble per unit time can be written as:

$$\dot{V}c = \eta \frac{A}{4} vc \tag{26}$$

Where c is the particle concentration, $A/4$ is the cross sectional area of the bubble.

If one assumes spherical particles and that particles removed pass within $r = R + a$, where a is the inclusion size. It can be shown that the collision efficiency can be expressed as:

$$\eta = \frac{3a}{R} \tag{27}$$

Given the very small carbide inclusion size of 0.1-5µm [2] the collision efficiency is expected to be low.

A crucial parameter for impurity removal through flotation is the size of the bubbles. As the removal of the carbide to the bubble takes place at the surface

of the bubbles, a large bubble surface area should be employed. In practice, this translates to minimising the size of the bubbles as the ratio of surface area and volume increases as the size of a bubble decreases.

5.3.6 Filtration

Filtration is defined as moving molten metal through a porous material to remove inclusions. In general, there are at least three participants in filtration: the molten metal, the filter material, and the inclusions to be removed. There are primarily two modes of filtration occurring:

1. Cake mode filtration
2. Deep bed mode filtration

In cake mode filtration, a layer, called a cake, of inclusions develops on top of the filter. The cake can lead to a significant pressure drop. An important aspect of cake mode filtration is that the cake is not only a result of the inclusion capture, but it is also responsible for capturing additional inclusions. [23]

Unfortunately, cake mode filtration does a poor job of capturing aluminium carbide inclusions as they are too small to be efficiently removed by the filter. [12, 27]

In deep bed filtration the inclusions are deposited on the walls within the filter, instead of being captured at the surface, as in cake mode filtration. To achieve good deep bed filtration a few issues need to be handled. Firstly, cake mode filtration needs to not occur, and they need to be deposited within the filter, thus the inclusions need to be sufficiently smaller than the pore size, so that the inclusions do not all get stuck on the surface of the filter. [23]

Bao proposed that during filtration, aluminium will expel inclusions with poorer wetting than the aluminium/filter interface. [30] So to achieve good removal of carbide inclusions, a filter material that wets aluminium better than aluminium wets the carbide should be utilised. Figure 12 shows the wetting behaviour of aluminium with a few possible filter materials.

It is evident that an alumina filter does not provide adequate wetting, to remove small carbide inclusions. While graphite provides the same wetting angle for the aluminium and carbide as for aluminium and the filter, [30] and is therefore better suited for removing the carbide. However, the graphite filter might also end up generating additional carbide. SiC has the best wetting angle with aluminium of the three filter materials and thus would be, the one best suited for removing

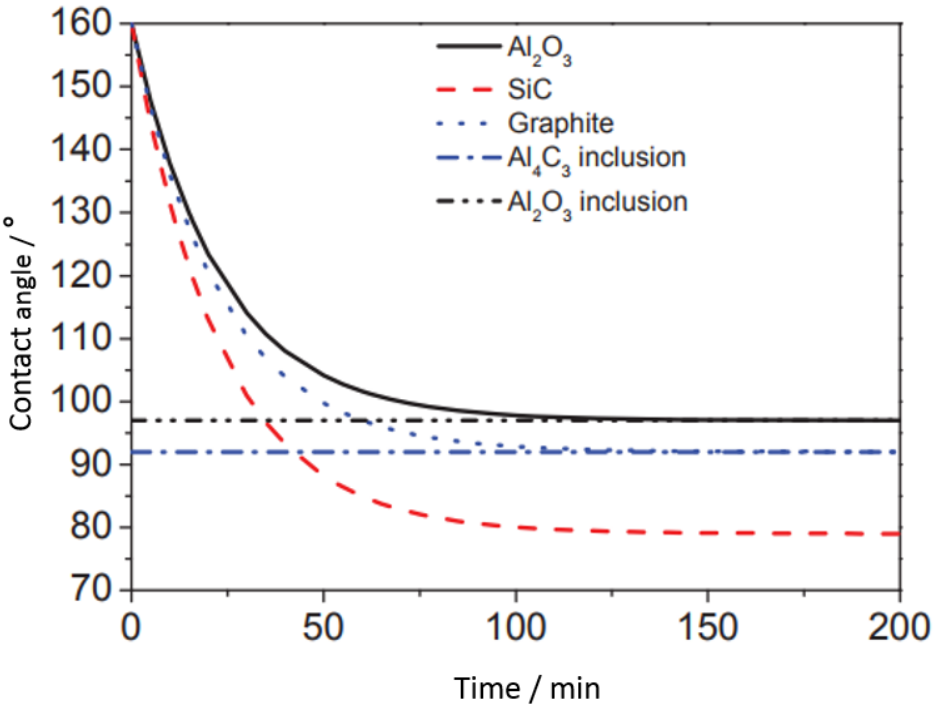

Figure 12: Contact angle of Al droplet on various ceramics at 700°C. [30]

the aluminium carbide, however it also might react with the aluminium forming additional carbide according to reaction 28. [34]

$$3\,\mathrm{SiC} + 4\,\mathrm{Al} = \mathrm{Al_4C_3} + 3\,\mathrm{Si} \tag{28}$$

But this reaction will not be very important for alloys containing large amounts of silicon as that will shift the equilibrium to the left favouring less carbide formation.

5.4 Model for refining in a batch reactor

Modelling the inclusion removal in a melt can give valuable information about the removal process. Such as the amount of inclusions remaining after a certain time or how great of an effect different parameters has on the process. Batch reactors are a commonly used type of reactor for refining operations. They also fit nicely with the experiments that was performed for this thesis. As the name implies this type of reactors handles a single batch of material at a time.

In general the mass balance required to derive equations describing a batch

reactor is obtained by equating the reduction of x to the amount of x transferred from the melt per unit time.

$$\frac{dc}{dt} = -\dot{Q} \tag{29}$$

Here c is the number of inclusions in the melt and $-\dot{Q}$ is the number of inclusions being removed from the melt per unit time.

Initially it can be assumed that inclusions are only removed by coming into contact with the bubbles rising through the melt. Then the amount of inclusions removed per unit time can be expressed as: [23]

$$\frac{dc}{dt} = -k_t \frac{A}{V} c \tag{30}$$

Where k_t is the mass transfer coefficient for removal to the bubbles, A is the surface area which inclusions are being removed to, and V is the volume of the melt.

By putting all factors dependent on c and t on separate sides of the equation and integrating it from the start concentration to the concentration after the refining, the following expression is obtained.

$$\int_{c_0}^{c} \frac{dc}{c} = -\int_{0}^{t} k_t \frac{A}{V} dt$$

$$\ln\left(\frac{c}{c_0}\right) = -k_t \frac{A}{V} t \tag{31}$$

Which can be rewritten as a decreasing exponential:

$$\frac{c}{c_0} = \exp\left(-k_t \frac{A}{V} t\right) \tag{32}$$

From this equation we can see that there are two parameters that determine the rate that inclusions are being removed at:

- k_t the mass transfer coefficient for removal to the bubble surface.
- $\frac{A}{V}$ the ratio between the area that is removing the inclusions and the volume of the melt.

The mass transfer coefficient k_t captures how efficient the mass transfer to the bubble surface and how efficiently the inclusions are removed once there, it is thus hardly surprising that it has a large influence on the removal.

The dependence on bubble area and melt volume is rather intuitive as a larger volume means that there is a larger amount of inclusions to remove in total. On the other hand a greater bubble surface area means a greater amount of the melt is being refined simultaneously.

The bubble surface area itself depends on several parameters. As previously mentioned the bubble size is the most important, smaller bubbles yields a larger specific surface area. Additionally it depends on the residence time of the bubbles, the residence time itself also depends on the size of the bubbles as smaller bubbles take more time to float to the surface. Equation (33) shows an expression for the bubble area.

$$A = \frac{3\dot{V}}{D}\tau \tag{33}$$

Where $\dot{V}$ is the volume flow of gas into the melt, D is the bubble diameter, and τ is the residence time of a bubble.

A similar approach can be used to derive an expression for the amount of inclusions remaining after refining when several removal mechanisms are considered. Starting with equation (29) the removal through each mechanism is summed up:

$$\frac{dc}{dt} = -\dot{Q} = -\frac{c}{V}(k_{tb}A_b + k_{tw}A_w + k_{ts}A_s) \tag{34}$$

Where k_{tb}, k_{tw}, k_{ts}, A_b, A_w and A_s are the mass transfer coefficients and areas of the bubbles, walls and, melt surface, respectively. Performing the same steps as was used to derive equation (32) yields the following expression:

$$\frac{c}{c_0} = \exp\left(-\frac{k_{tb}A_b + k_{tw}A_w + k_{ts}A_s}{V}t\right) \tag{35}$$

This however assumes that all the inclusions are of the same size, which they are not, in section 5.2.3 it was established that the inclusion size follows a decreasing exponential distribution. Additionally the mass transfer coefficients are dependent on the size of the inclusion being removed. To account for this equation (35) must be rewritten to:

$$\frac{f_N(r)}{f_{N_{in}}(r)} = \exp\left(-\frac{k_{tb}(r)A_b + k_{tw}(r)A_w + k_{ts}(r)A_s}{V}t\right) \tag{36}$$

By assuming the inclusions to be spherical and multiplying with the inclusion-volume followed by integrating both sides from $r = 0$ to $r = \infty$ an expression for the inclusion volume can be obtained.

$$c_V = \int_0^\infty f_N(r) \frac{4\pi r^3}{3} \exp\left(-\frac{k_{tb}(r)A_b + k_{tw}(r)A_w + k_{ts}(r)A_s}{V} t \right) dr \tag{37}$$

From this it can be determined that the most important parameters for inclusion removal is:

- The bubble size, because a larger specific bubble area enhances the removal rate.
- The mass transfer coefficient, unfortunately it can be extremely challenging to obtain expressions for the mass transfer coefficients as they may vary significantly between setups.
- The size distribution of inclusions, however the inclusion amount is what is being refined in the first place.

6 Experimental

6.1 Experimental matrix

Experimental matrix, displayed in table 1, was designed to investigate the effect of temperature, remelting, water content and bubble size. Because previous experiments had shown that water in Ar gave the greatest reduction of carbide content it was the only reactive gas investigated. But water is also a safety hazard, and something that is typically not wanted close to liquid metal, so a lower water content than used previously was also investigated.

Table 1: Table shows number of experimental parallels for each parameter.

	700°C	750°C	800°C
Remelting	4	3	4
2% H_2O	3		
1% H_2O	3		

	1100°C
Carbide formation	7

In total three different setups were used:

- Remelting experiments were performed in a closed induction furnace.
- Gas injection experiments using moist argon were performed in an induction furnace closed through using an external hood.
- The carbide formation experiments were performed in a resistance heated graphite tube furnace.

6.2 Characterisation of samples from preliminary work

From earlier work performed by the author samples with a very high carbide content of roughly 3000ppm were obtained. The samples were produced in an experiment were argon with 10% CO_2 were blown through molten aluminium for 30 minutes at 800°C. The experiment yielded metal with 7.7ppm carbide and a dross layer with roughly 3000ppm aluminium carbide. [1] The sample was polished and examined in a SEM using a secondary electron detector and EDS.

6.3 Carbide formation experiments

6.3.1 Materials

The materials used were 99.999% pure aluminium pellets, while carbon was supplied from a graphite crucible.

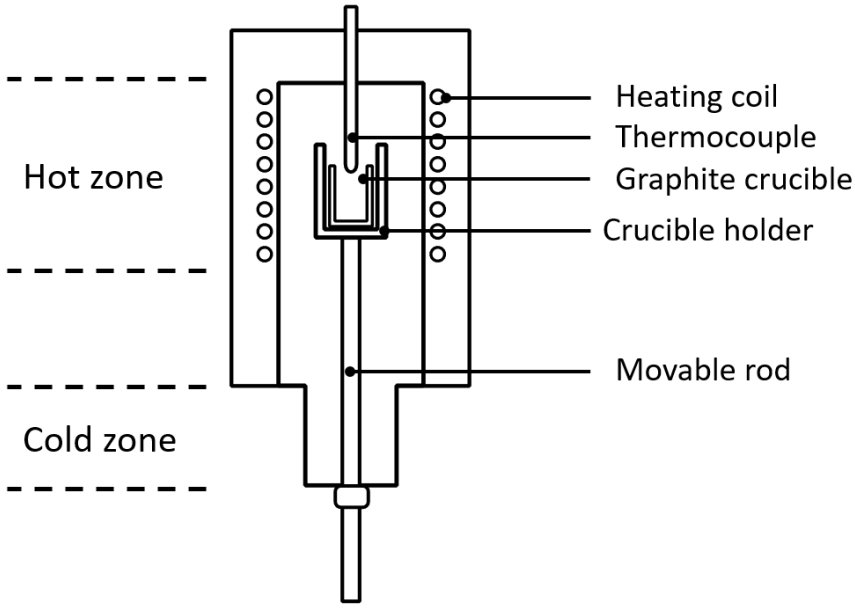

Figure 13: Setup for the carbide formation experiments.

6.3.2 Setup

The experiments were performed in a resistance heated graphite tube furnace. To prevent air from contaminating the experiment the furnace was flushed with argon and kept at a slight over-pressure of 1.1bar to 1.2bar. The furnace had a retractable rod which allowed moving the crucible from the cold zone at the bottom of the furnace to hot zone at the top. A schematic setup of the furnace is displayed in figure 13.

6.3.3 Procedure

During each experiment the furnace was heated to 1100°C. Once at that temperature the crucible was moved from the cold zone into the hot zone through use of the retractable arm. Then the crucible was left there for 5 hours before the furnace

was switched off and the crucible moved back into to the cold zone, and retrieved from the furnace when it was cold enough to handle.

Experiments were performed at 1100°C to make sure that the protective alumina layer was removed completely allowing the interaction between aluminium and carbon to be observed rather than the interaction between alumina and graphite.

After being removed from the furnace the samples were quickly cast into epoxy to shield them from humid air. To prevent the samples being electrically charged while they were examined in the SEM, carbon tape touching the edge of the droplet and another piece attaching the sample to the sample holder. The two pieces of carbon tape was connected with aluminium foil to allow charge to leave the sample.

6.4 Remelting experiments

6.4.1 Materials

The raw material was electrolysis aluminium supplied by Hydro, with a carbide content in the area around 30-40ppm. In total 40kg of metal was supplied. The metal had to be cut into smaller pieces to fit inside of the crucible. During cutting, a water cooled saw was used. The carbide analysis of the metal found a carbide content of 34.5ppm.

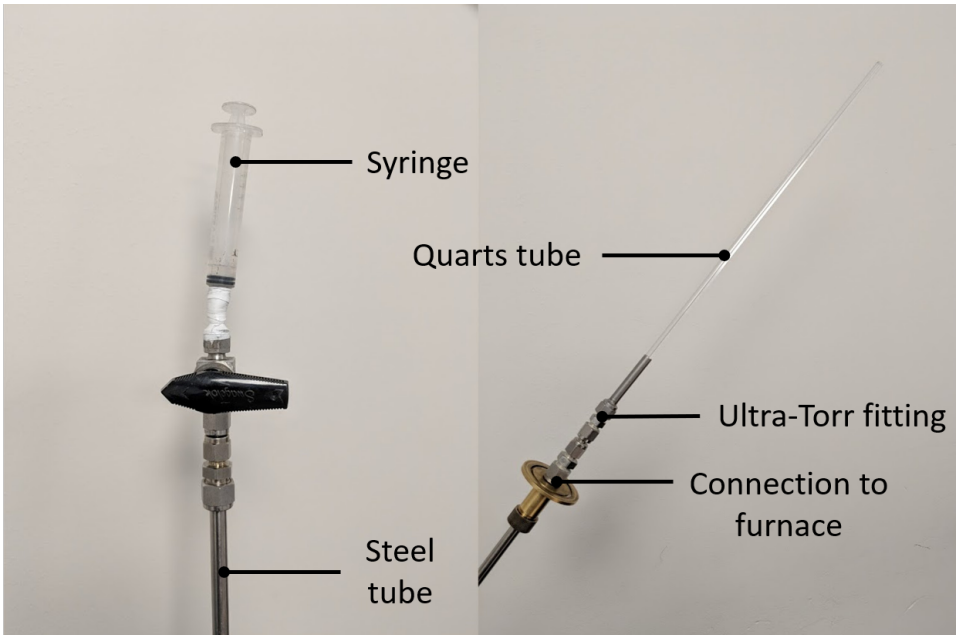

Figure 14: Sampling device used for retrieving samples in situ.

6.4.2 Set-up

In each experiment a sintered alumina crucible was placed within a graphite crucible, an alumina tube was placed against the inside wall of the alumina crucible to hold the thermocouple. Then the crucible were charged with approximately 200g of aluminium, before being placed inside of the furnace.

Samples were taken by inserting a sampling device through the top of the furnace. Before insertion the sampling device was placed in an intermediary chamber connected to the furnace which could be evacuated and flushed with argon.

The sampling device is displayed in figure 14. It consists of a steel tube which is connected to a syringe in one end and a quartz tube in the other. To make it simple to exchange the quartz tube between samples a cable gland was used to connect it to the steel tube.

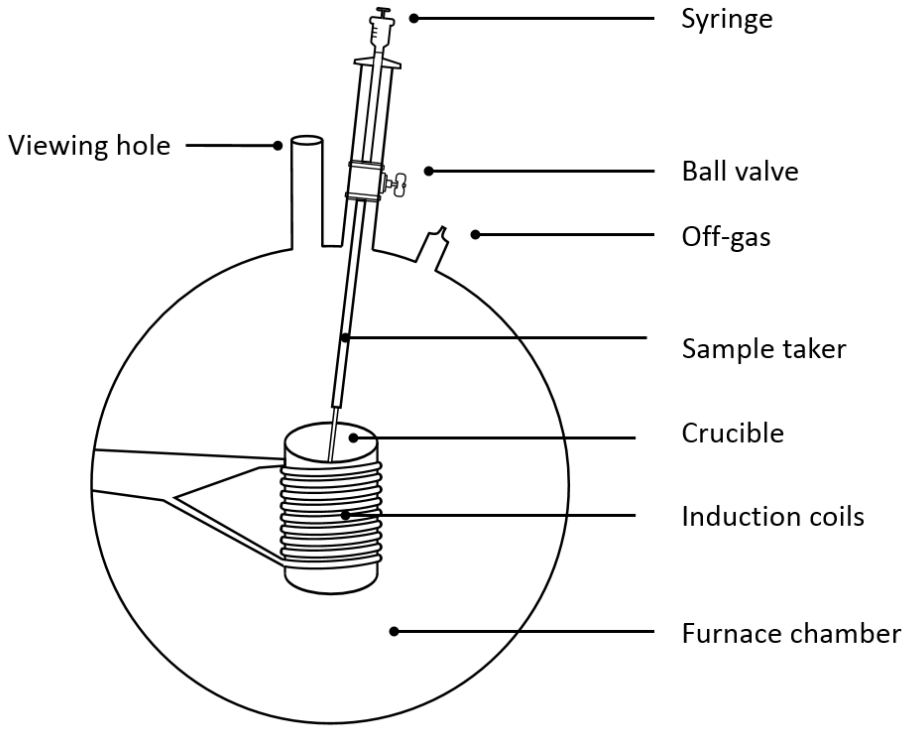

Figure 15: Experimental setup for the remelting experiments.

6.4.3 Furnace

The experiments were performed in an induction furnace closed off from the surrounding atmosphere. It was equipped with several viewing holes to make it possible to observe the crucible during an experiment. Additionally it also had an opening to take samples in situ. To prevent air from getting into the furnace an intermediary chamber that could be closed of from the main furnace chamber with the help of a ball valve, was connected to the opening. The intermediary chamber was also connected to the vacuum pump and argon supply to prevent air from contaminating the experiment after exchanging quartz tube. An image showing the furnace setup is displayed in figure 15.

6.4.4 Procedure

After the crucible was inserted into the furnace, the furnace was evacuated and flushed with argon two times. Then the furnace was heated until the thermocouple read approximately 750°C and kept at that temperature until melting began. As the metal melted the temperature reading rapidly dropped to the melting point and remained there until it was completely molten, afterwards the melt was heated to the holding temperature of the experiment. Upon reaching the holding temperature the first sample was taken, and after being held at that temperature for 30 minutes the second sample was taken. Then the power was switched off and the metal was allowed to cool down before being retrieved from the furnace.

6.5 Gas injection experiments

6.5.1 Materials

The raw material was the same as used for in the remelting experiments, see section 6.4.1.

6.5.2 The hood

To shield the melt from the outside atmosphere a specially designed hood, displayed in figure 16, was made to fit on top of the furnace.

The hood consisted of two cylindrical shells. There was a flat surface between the two rings that contained an opening to retrieve samples during experiments, inlet for the argon gas that was blown on the surface of the melt, outlet for off-gas, and a viewing port. A steel rod connected to an alumina rod connected to an alumina filter was inserted through the top of the hood. Holders for thermocouples

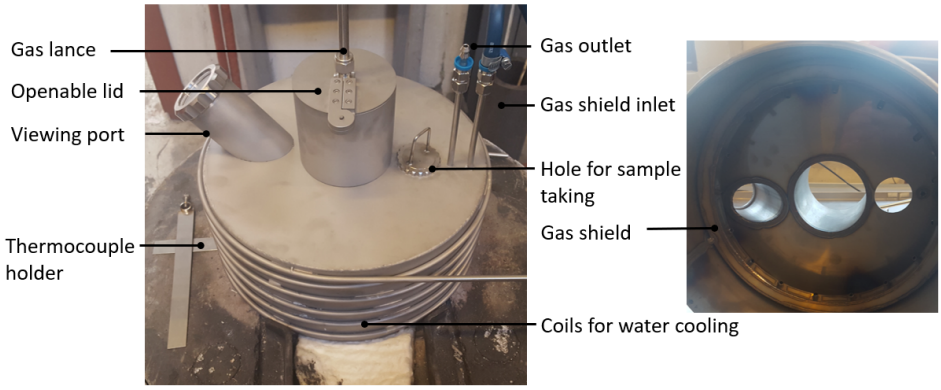

Figure 16: Hood used to close the furnace, diameter is 310mm.

was placed between the hood itself and furnace. To prevent leaks gaskets were placed between the hood and thermocouple holders, and between the furnace and thermocouple holders.

6.5.3 Sampling device

Samples were taken during the experiment through a hole in the hood. Because the sampling device used during the remelting experiments produced poor quality samples, which were too small and had many shards of glass stuck in the metal, a new on had to be built.

The new sampling device consisted of a quarter inch steel tube connected an alumina tube using a Swagelok Ultra-Torr fitting. To suck the metal into the alumina tube a peleus balloon was connected directly on to the other side of the steel tube. The new sampling device produced much better samples than the previous one, the sample mass was greater than 2g and aside from the very tip they were free of alumina shards. After a sample was taken it was retrieved by shattering the alumina tube with a hammer. A picture of the sampling device and an a sample retrieved by it is displayed in figure 17.

6.5.4 Humidification set-up

To humidify the argon it was blown through a water bottle. Shortly before it was blown into the hood the relative humidity and temperature was measured with a probe. A transparent tube was attached just before the humidity sensor to make sure that no condensation occurred. The water content of the argon was adjusted

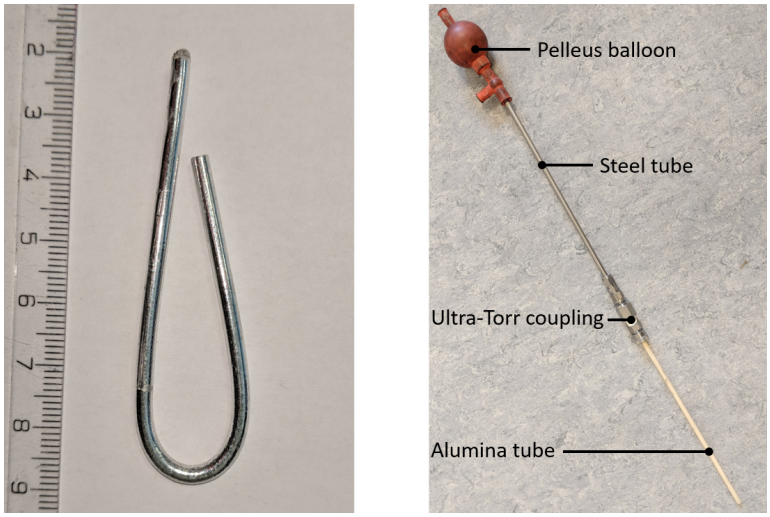

Figure 17: Example of a sample obtained using the newer sampling device, as well as the sampling device itself.

by altering the temperature of the water within the water bottle. To cool it down, thus reducing the water content, it was placed in an icebox filled with crushed ice, and to increase the water content the bottle was placed on a hot plate. Schematic drawing of the humidification setup is shown in figure 18.

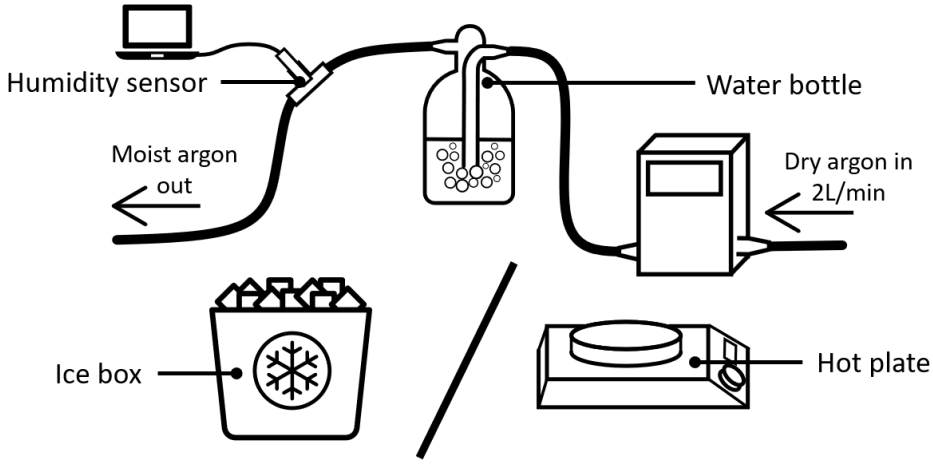

Figure 18: Schematic drawing of the humidification setup, a hot plate or ice box is used to change the water temperature.

To add 2% water to the argon it was sufficient to just leave it out in the room

which had a temperature of around 28°C, with occasional cooling. While adding 1% water required the bottle to be cooled continuously with occasional heating.

6.5.5 Gas lance

The gas lance was made from an alumina rod which was glued to an alumina filter using CALDE TROWEL HF 36 U, which is comprised predominantly of alumina and silica. The other end of the alumina tube was attached to a steel rod using a Swagelok Ultra-Torr fitting. During the experiments the O-ring that was used in the fitting melted, however it seemed to last the duration of the experiment. After an experiment what was left of the O-ring was scraped out and replaced with a new one.

6.5.6 Crucible

The crucible consisted of two layers: An outer graphite layer which provided structural integrity and a flat bottom the crucible could rest on, and an inner layer made from 92% alumina and 7% silica. Each layer was its own crucible which was glued together with CALDE TROWEL HF 36 U. Figure 19 shows the different layers that crucible was comprised off.

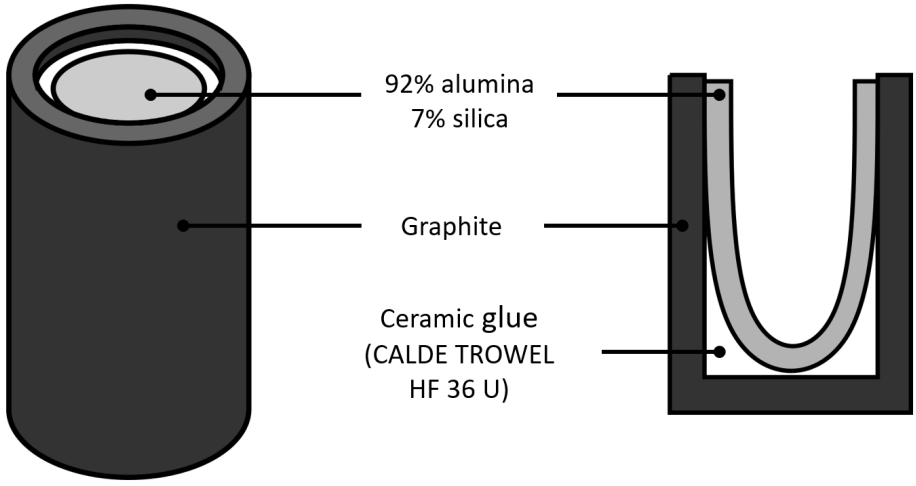

Figure 19: Different layers of the crucible used during the gas injection experiments.

An issue which arose was that despite the two crucibles being glued together 2 weeks prior to the experiments taking place, they produced a lot of steam, methane

and CO during heating. To limit the influence this would have on the experiments the temperature was held relatively low until the FTIR could verify that no more gases were being produced.

6.5.7 Set-up overview

The main parts of the set-up was the induction furnace, the hood placed over it, and the FTIR used for analysing the off-gas. Argon was supplied from a bottle and split off in a T-junction, where tube went to the gas shield and the other went to the humidification set-up. Two mass flow controllers were used to control the volume flow of gas. A flow of 10NL/min was used for the gas shield during the experiments, while 2Nl/min was sent through the humidification set-up during the refining period.

The gas which went into the FTIR was sampled from the top of the hood, the FTIR only needs 2.5Nl/min so the rest of the gas was sent directly to the ventilator. Before being sent into the FTIR the gas was sent through a bottle to remove excess water and then through a heated tube.

A schematic drawing of the setup is displayed in figure 20.

6.5.8 Procedure

Before each experiment the crucible, gas-lance and thermocouple tube were coated with boron nitride so the molten aluminium would not stick. Then roughly 1kg of aluminium was inserted into the crucible followed by the crucible being placed inside the furnace. To raise the crucible a graphite brick was placed underneath it so that there was a good view through the viewing hole in the hood. Then the hood was placed over the furnace and leaks were closed as well as possible and argon was purged through it at a flow of 10L/min, the off-gas composition was monitored by the FTIR. While purging the volume percent of oxygen was reduced to 4-6%.

After purging the furnace was turned on and the metal was heated till it melted, then the power was reduced to make sure that the temperature would not rise above the target of 700°C. After the metal was molten and the temperature reached 700°C the furnace was switched off and the first sample was taken. Then the furnace was switched back on, and moist argon was blown through the lance at a flow of 2L/min.

To control the amount of water that was added to argon the water temperature in the water bottle could be adjusted through placing it in an ice box or on a hot-plate. However the hot plate was not much needed because the sunny weather ensured the room was quite warm.

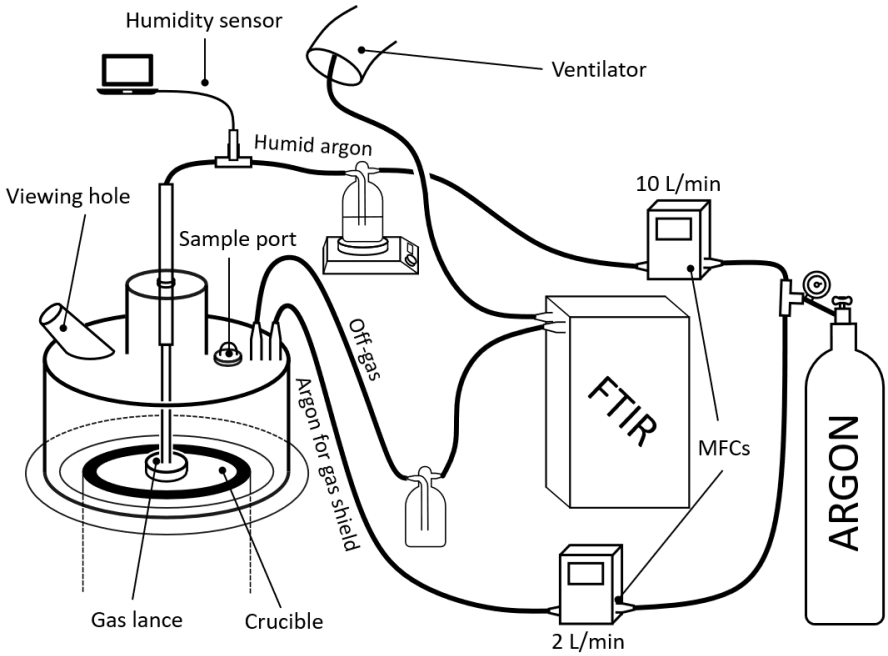

Figure 20: Schematic drawing showing all the different parts of the setup and how they are connected together.

Once the off-gas had reached a stable composition, and the water content of the moist argon had reached the desired level, the lance was submerged in the melt and held there for 30 minutes. After the holding time the lance was withdrawn from the melt and the second sample was taken. The remaining metal was cast into a graphite mould. A dross sample was taken from the material that was stuck to the filter as it was pulled out.

6.6 Sample analysis

6.6.1 Preparation for microscopy

A special procedure had to be used to prepare the samples for microscopy. Because aluminium carbide reacts with water, including normal air humidity, they needed to be protected during and after polishing. To achieve this the samples were polished in high purity mineral oil. After the polishing they were stored in a closed vial filled with additional mineral oil.

Before the samples can inserted into the SEM all the oil must be removed,

because an oily sample would damage the SEM, and because achieving a vacuum would not be possible. Roughly 15 minutes before the samples were inserted they were thoroughly washed with heptane to remove all the mineral oil. Each sample was washed until they no longer left a greasy mark on tissue paper after being wiped. Porous samples were placed in a vacuum chamber for a few minutes to remove heptane that was trapped within the porous regions of the sample. In the SEM the samples were imaged using a secondary electron detector and regions containing carbide was identified using EDS. Images are displayed in the results section.

6.7 Analysis methods

6.7.1 FTIR spectroscopy

The main principle behind fourier transformed infrared (FTIR) spectroscopy is that molecules can absorb electromagnetic radiation in the infrared range, and that the amount of radiation absorbed changes with the wavelength of the light. The simplest and most straightforward way to obtain a spectrum would be to shine monochromatic light at the sample and measure how much light is absorbed, and then repeat for several different wavelengths. FTIR spectroscopy is a more sophisticated approach, instead of using monochromatic light, a light source shining many different wavelengths is used. Then the beam is altered so it contains different wavelengths yielding another datapoint. After being repeated many times a fourier transform is used to calculate the amount of light that is absorbed at each wavelength. [35]

Whenever the frequency of the infrared light is the same as vibrational frequency of a bond it is absorbed. Because different molecules contain different amounts of bonds and types of bonds they will produce different absorption spectra. Through comparing the absorption spectrum obtained from the sample with reference spectra it is possible to determine the composition of the sample gas.

A limitation with FTIR spectroscopy is that absorption will only happen if there is a change in dipole moment. [35] As a result it is impossible to use this technique to analyse for H_2 N_2 or O_2. So any of the reactions mentioned in section 5.3.6 releasing hydrogen can't be detected.

A large advantage from using FTIR to produce as a spectrum is the speed. [35] Instead of recording the absorption at each point separately using a dispersive instrument, FTIR spectrometers obtain absorption at all the different wavelengths

simultaneously. By requiring less time to gather the data it is possible to get a more detailed view of the changes happening during an experiment.

To obtain the composition of the gas which is being analysed the spectrum obtained by FTIR spectroscopy is compared to a reference spectrum of a gas of known composition. If the reference spectrum contains all the features that was found in the spectrum of the sample gas, there is no residual and the composition matches the reference gas. If the sample gas contains several different gas species obtaining its composition gets more difficult. As spectra start overlapping it becomes more difficult to determine the composition accurately. To avoid this problem the models being used to analyse the data only use parts of the spectrum, which have been selected to minimise overlap. Some gases are particularly difficult, for example water vapour, because it takes up a large part of the spectrum which gives it a greater chance for interfering with other species contained by the sample gas.

6.7.2 Carbide analysis

The sample analysis was carried out through gas chromatography by Hydro, see references for a more in depth description of the method. [2] Each sample was cleaned and placed in the reaction bulb, which is shown in figure 21, it was then evacuated to a pressure of 10^{-5} torr. Then hot sodium hydroxide was added to dissolve the sample. Aluminium carbide will decompose in contact with water and form methane:

$$\mathrm{Al_4C_3} + 12\,\mathrm{H_2O} = 3\,\mathrm{CH_4} + 4\,\mathrm{Al(OH)_3} \tag{38}$$

After the reaction is finished, 5 ml of the gas is removed through the septum with a syringe and injected into the gas-chromatograph. Then by utilising the ideal gas law, the amount of carbide is calculated by comparing the methane peak with the peak of a reference gas with a known methane content. [2]

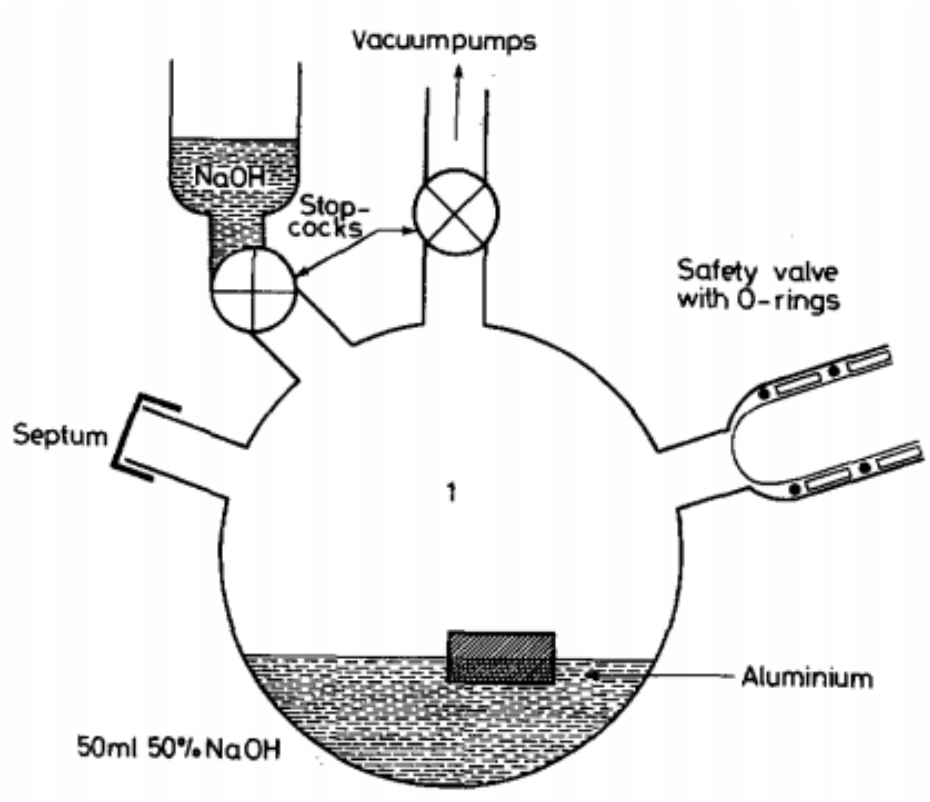

Figure 21: Glass bulb for dissolution of the metal samples. [2]

7 Results

7.1 Preliminary results

Preliminary experiments were performed with various experimental parameters. Samples with a very high carbide content of 3000ppm was analysed metallographically. SEM images of the samples are displayed in figure 22, 23 and 24. The particles scattered across the surface of figure 22 has a size consistent with previously reported aluminium carbide particle sizes, 0.5µm - 5µm. [2, 1]

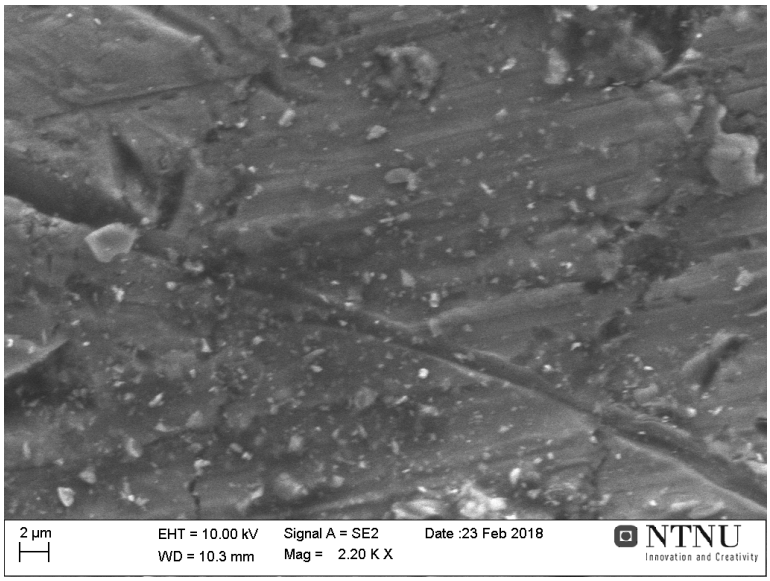

Figure 22: SEM image of dross sample with a large amount of carbide particles, before EDS.

After doing chemical analysis with EDS the spots which were analysed reacted leaving small particles behind. Figure 23 shows the same region as figure 22 but imaged after EDS analysis was performed. Furthermore one can see that the surrounding region of the particles is much darker and seems to be mostly free of the aluminium carbide particles. This may be related to the samples being polished in oil, and the electron beam heating up the sample during the EDS point analysis which cause the oil to be ejected from pores on the sample surface.

Two samples taken from the same experiment were examined which revealed the material to be very inhomogeneous. Comparing figure 22 with figure 24 reveals a much lower density of carbide particles in the second sample. While it is not

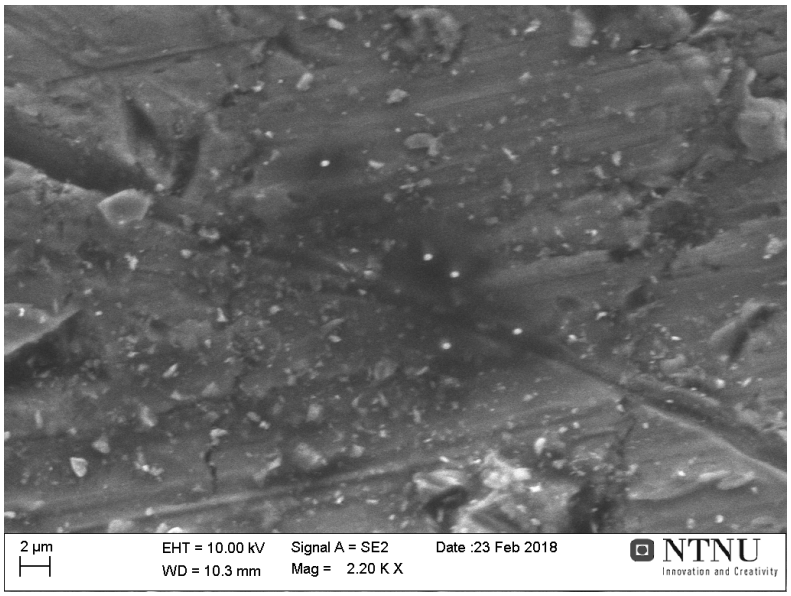

Figure 23: SEM image of dross sample with a large amount of carbide particles, after EDS.

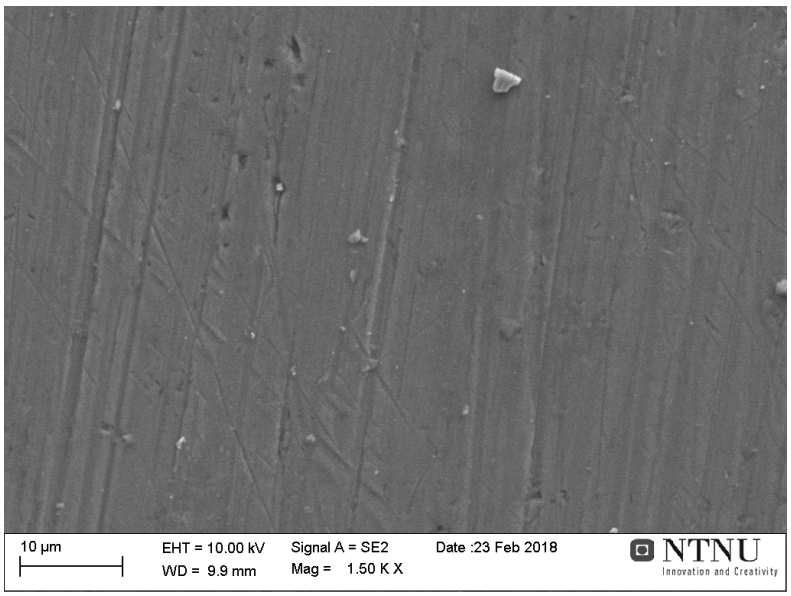

Figure 24: Different sample from the dross with 3000ppm carbide, but a region without many carbide particles.

unexpected that the dross material is inhomogeneous it leads to large variance in successive measurements made on dross samples.

7.2 Carbide formation

Inspecting the aluminium droplet which was kept at 1100°C for 3.5 hours in a graphite crucible revealed a carbide layer to have formed on the sample surface. The carbide layer was continuous covering the whole surface of each sample. Figure 25 shows a SEM picture of the bottom of a sample in the region were they stop contacting the crucible.

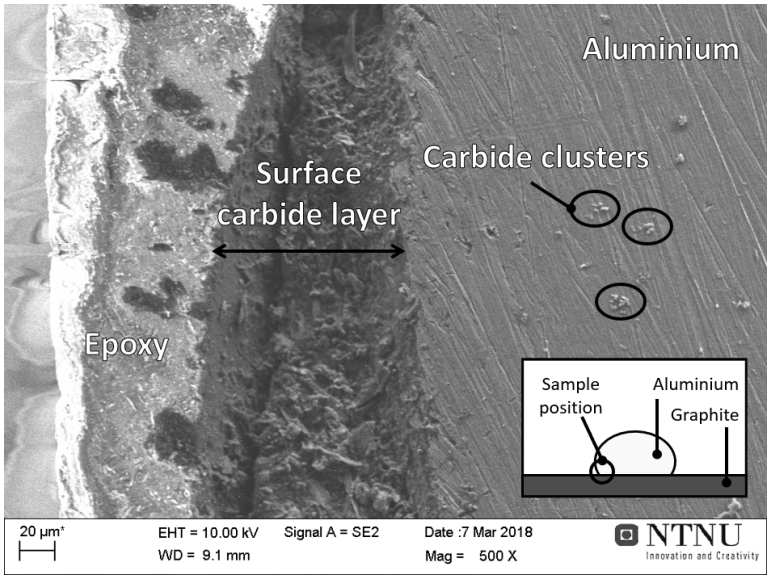

Figure 25: Cross section of the bottom of the droplet, area was in direct contact with the graphite crucible, 500x.

The SEM pictures reveal that the region of the sample which contacted the graphite crucible had a carbide layer that was many times thicker than the remaining surfaces of the sample, see figure 25.

In close proximity to the surface large carbide clusters were found. The distribution of carbide particles was in-homogeneous, some regions had a high density of carbide particles while other regions had almost no carbide present aside from the surface layer. Further towards the centre of the sample the amount of carbide was significantly reduced, figure 27 shows a typical image of the centre of a sample.

It is also evident how rapidly the carbide reacts with the humidity in the air.

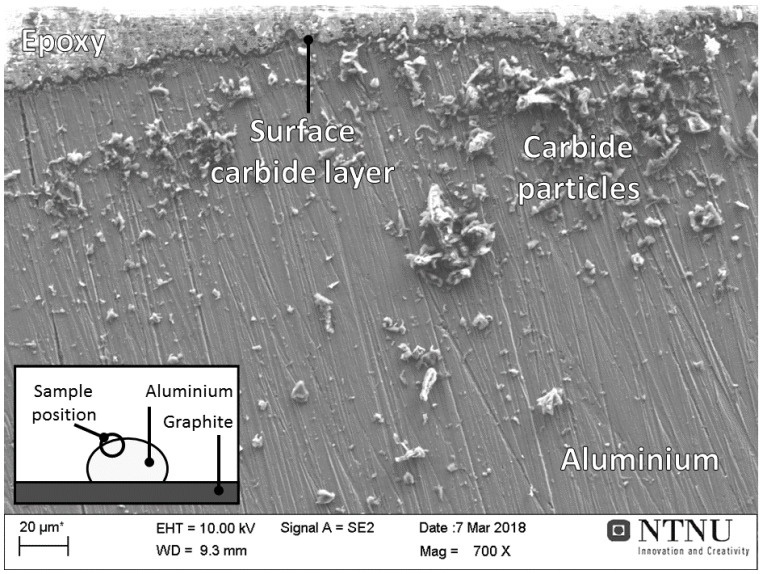

Figure 26: A large carbide cluster close to the edge of the sample.

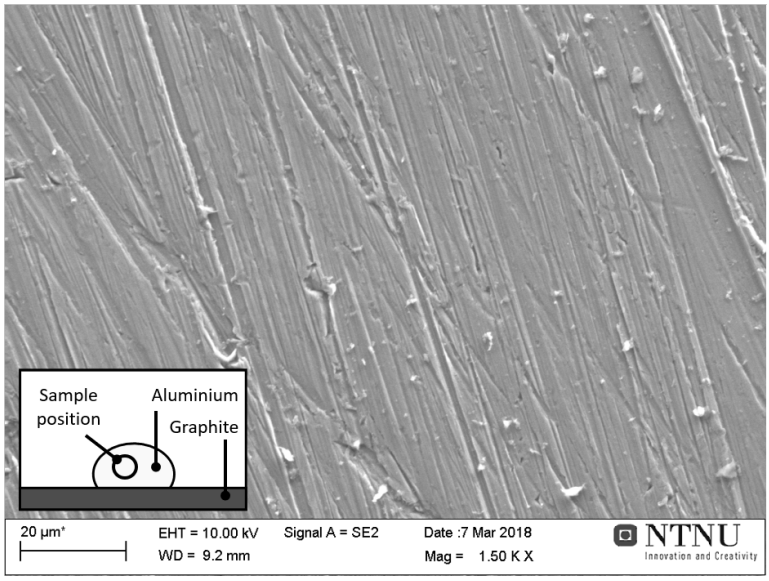

Figure 27: Image of the interior of the sample, low amounts of carbide particles found away from the surface.

Figure 25 shows that after the sample has been exposed to the atmosphere for only 20 minutes, one can already see the carbide layer has deteriorated a fair amount during this short time span.

7.3 Remelting experiments

The remelting experiments had samples from the dross and from the bulk metal analysed after being held for 30 minutes at the desired temperature, the analysis results are shown in table 2. The samples retrieved in-situ by using a sampling device was of poor quality, they had too low mass and glass shards stuck to the metal, so they could not be analysed. Instead samples was taken through use of a handsaw from the surface and middle section of the melt after it had solidified in the crucible. The first parallel at 750°C, appears to be an outlier as it has a much higher carbide content than the other experiments performed at the same temperature.

Table 2: Carbide content from the remelting experiments.

	Al_4C_3 content / ppm	
Experimental parameters	Metal	Dross
Remelt @ 700°C parallel 1	7.1	15
Remelt @ 700°C parallel 2	2.6	17
Remelt @ 700°C parallel 3	2.1	5.2
Remelt @ 750°C parallel 1	-	25
Remelt @ 750°C parallel 2	4.6	29
Remelt @ 750°C parallel 3	2.5	9.1
Remelt @ 800°C parallel 1	5.2	7.1
Remelt @ 800°C parallel 2	8.4	13
Remelt @ 800°C parallel 3	12	17

7.4 Gas injection experiments

In the gas injection experiments samples were taken from the bulk metal right after the metal melted, after 30 minutes, and from the dross after 30 minutes, the results are shown in table 3. During each of the experiments a dross layer enriched with carbide formed, while the carbide content of the metal was reduced significantly. In previous experiments the carbide content of the metal was found

to be very homogeneous, thus only a single metal sample was analysed for each experiment; while some of the experiments had two dross samples analysed. The carbide content of the dross proved to be very inhomogeneous, with two samples from the same experiment varying by more than 400%.

Table 3: Carbide content from the experiments with moist argon.

	Al_4C_3 content / ppm				
Parameters	Start sample	After 10 min	After 30 min	Dross 1	Dross 2
1% H_2O parallel 1	5.6	-	4.2	224	-
1% H_2O parallel 2	7.9	-	-	255	142
1% H_2O parallel 3	8.6	-	2.4	221	964
2% H_2O parallel 1	4.7	-	1.8	40	-
2% H_2O parallel 2	-	1.8	-	274	250
2% H_2O parallel 3	9.0	-	2.5	126	110

Observations from the experiments:

- During the experiments the O_2 amount detected in the off-gas was at around 4%.
- While gas was being blown through the melt faint orange flames could be seen above the melt surface.
- The ceramic glue that was used to make the crucible and lances released a lot of water vapour during the first experiments it was used in, despite being prepared several weeks in advance. The water was released at around 500°C. To prevent this from having too large an effect on the results the temperature was held steady below the melting point until no more water was detected in the off-gas. The experiments which were influenced by this are parallel 1 and parallel 2 with 2% H_2O.
- Some soot formed during the experiments, on the inside of the crucible and on the tip of the lance itself.

Dross samples taken when 1% and 2% water was added to the argon were examined in a SEM. Carbide particles were identified using EDS. Large amounts of carbide particles were found scattered all over the surface. Most of the surface of the samples had an even distribution of carbide particles, but it was also possible

to find clusters of carbide, similarly to what was found in the carbide formation experiments. It was no significant differences between the different samples that were analysed. Figure 28 displays two typical carbide clusters next to each other, one with small particles from 0.5µm - 1µm, and one with medium sized carbide particles from 1µm - 3µm. The results closely resemble previously reported values. [2, 1]

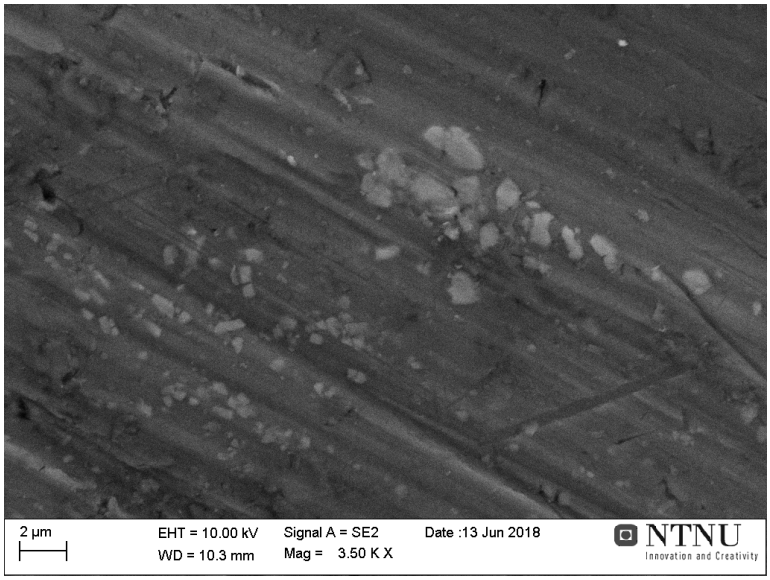

Figure 28: Carbide cluster found in the dross collected after blowing humid argon through the metal for 30 minutes.

The off-gas was analysed for the experiments were a reactive gas was used. The instrument used to analyse the off-gas was an FTIR-spectrometer. While the FTIR can detect a wide variety of gases only CO, CO_2, CH_4, and H_2O were examined, O_2 was examined with a separate oxygen detector the FTIR was equipped with. Unfortunately the instrument is incapable of detecting H_2.

Observations made on the off-gas analysis, figure 29, 30, 31 and 32:

- The setup was able to reduce the amount of O_2(g) to 4%, even after opening the sample hole the amount of O_2(g) didn't increase significantly.
- The CO_2 remained steadily at around 0.1% to 0.2% most of the time with occasionally higher amounts, which seemed to be triggered by the CO(g) content increasing. Expected to happen because of the Boudouard reaction.

- Right after the lance was submerged in the molten aluminium both the CH_4(g) amount and CO(g) amount increased. Similar to what was observed in the preliminary results. [1] Additionally it can be seen that when a large amount of methane is produced a large amount of CO(g) forms as seen in figure 29 and 31, similarly when a lesser amount of methane is formed a lesser amount of CO(g) forms, as seen in figure 30 and 32.
- The CH_4 peak lasted only a short amount of time, after 10 minutes CH_4 was no longer formed in any significant amounts.

Unfortunately some errors occurred while performing the experiments.

- Two of the experiments got contaminated with carbon, which lead to an increase in carbide, those results have been removed. The contamination most likely originated from the graphite wool surrounding the crucible, or the outer crucible itself as it is made of graphite.
- The second parallel with 2% H_2O had an error with the sampling device so the first sample was taken 10 minutes after the lance was submerged instead of right before.

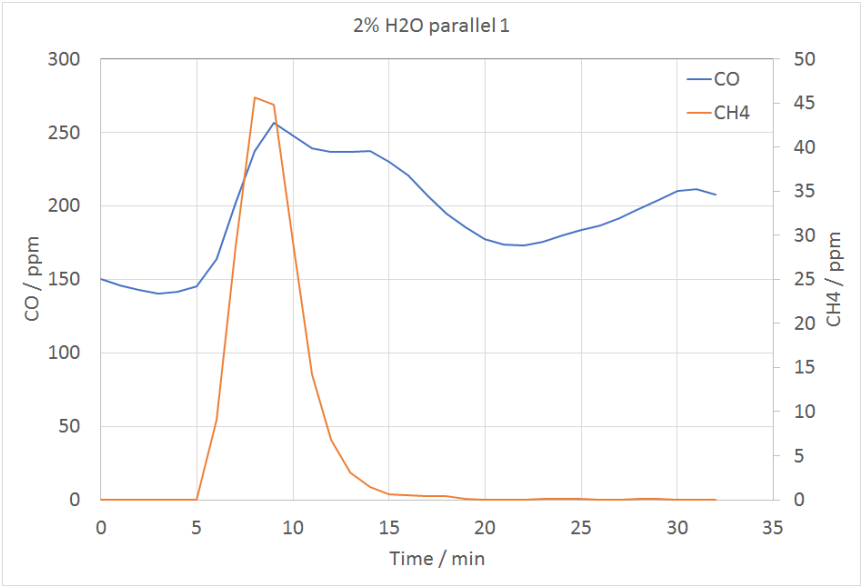

Figure 29: CO(g) and CH_4(g) content of the off-gas in parallel 1 when 2% H_2O was added to the purge gas.

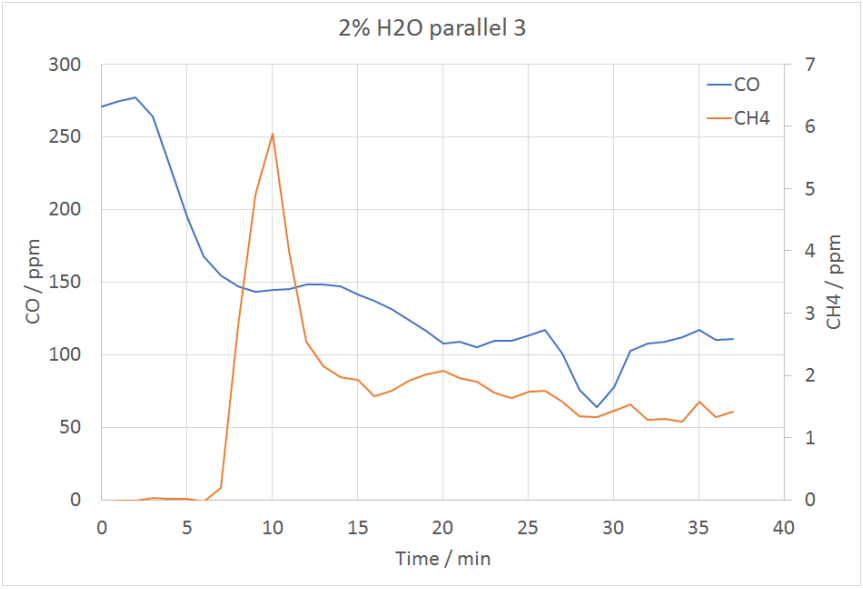

Figure 30: CO(g) and CH_4(g) content of the off-gas in parallel 3 when 2% H_2O was added to the purge gas.

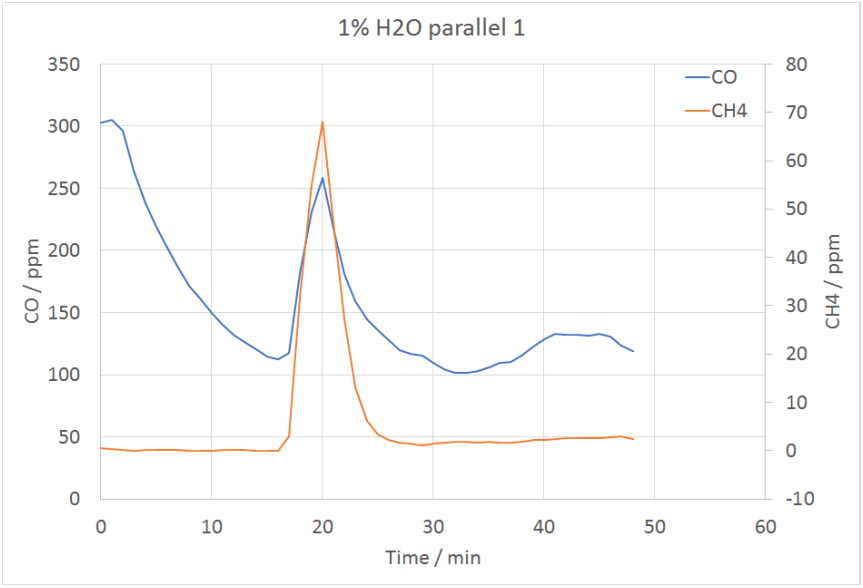

Figure 31: CO(g) and CH_4(g) content of the off-gas in parallel 1 when 2% H_2O was added to the purge gas.

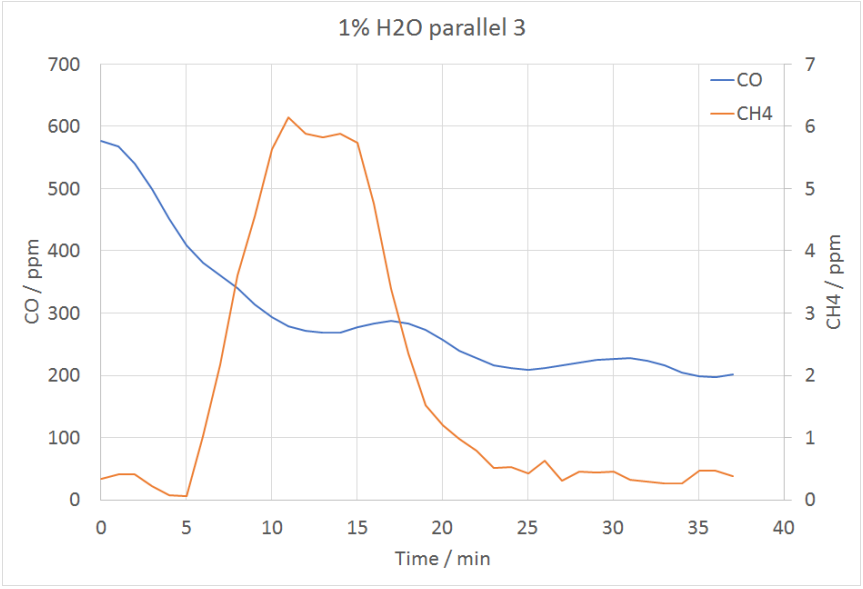

Figure 32: CO(g) and CH_4(g) content of the off-gas in parallel 2 when 2% H_2O was added to the purge gas.

8 Discussion

Ideally the experimental results could be examined in the same fashion as during the preliminary studies. There an experiment with no gas injection was performed and used to get an idea for how much carbide was removed due to only remelting, so the other effects could be more easily isolated. [1] But unfortunately it was not enough time to perform remelting experiments in the setup the gas injection experiments were done in. An online sample was taken before gas injection to show the remelting effect, and another online sample after the gas injection which shows the sum of the remelting and gas injection effects. Instead one can compare the amount of carbide right after melting to the amount remaining carbide after injecting the reactive gas into the melt, as in equation 39.

$$\text{Removal efficiency} = 1 - \frac{\text{End sample}}{\text{Start sample}} \tag{39}$$

Unfortunately only three parallels were performed for each set of parameters, additionally two experiments produced no results, meaning that there is a significant amount of uncertainty with the results. However, the results that were collected is displayed in figure 33. The results from when 1% H_2O was used have one measurement with very low carbide efficiency unlike when 2% was used, but there are insufficient measurements to determine if the difference is due to the different H_2O content or just variance between the different parallels.

8.1 Comparison between setups

Figure 34 shows a comparison between the results from the two current setups used and the one used in the preliminary experiments. The figure shows that the remelting setup that was used performed about as well as the one used in the preliminary experiments, on the other hand the setup used in gas-injection experiments did not perform as well.

The biggest difference between the setup used during the preliminary work and the gas injection setup was the amount of oxygen present. The large pouring spout on the furnace which was used proved difficult to seal and was likely the main source of outside atmosphere entering the hood. The outside atmosphere entering the hood might be the reason flames were seen above the melt during purging as the methane burned after leaving the melt. Another key difference is that in the preliminary experiments all the carbon that was present had been covered up with

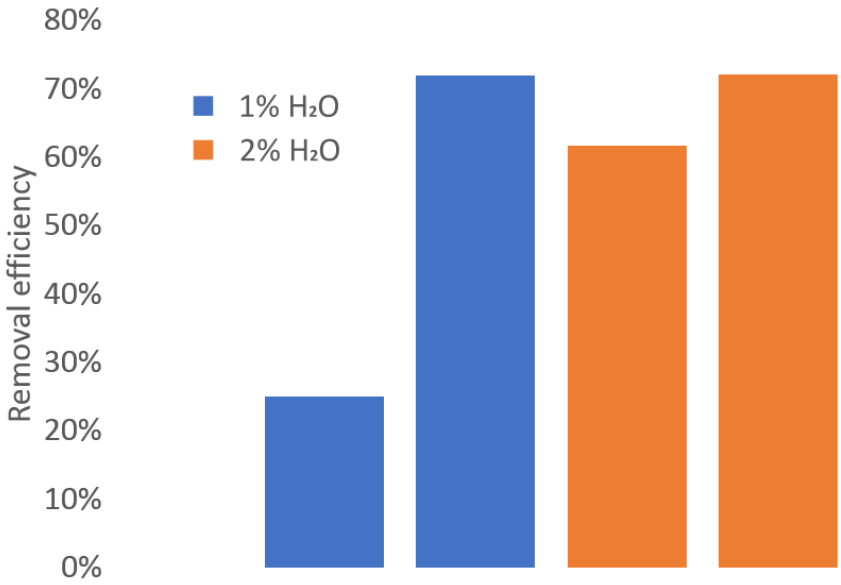

Figure 33: Removal efficiencies of the gas injection experiments.

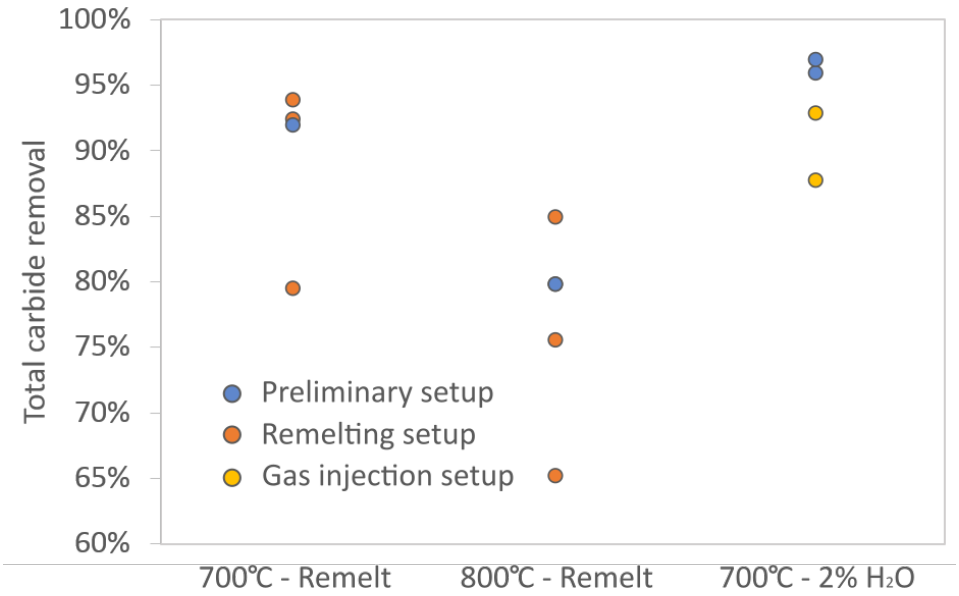

Figure 34: Comparison of carbide removal for the various setups used.

alumina powder and ceramic wool. This is probably the reason so much less soot was formed during the preliminary experiments.

The remelting experiments had no outside atmosphere present because it was fully evacuated and filled with argon before the experiments begun. However, there were carbon present from the outer crucible, and the graphite wool it was wrapped with. Some soot was formed on the alumina crucible, but the results indicate that the soot was not able to penetrate the melt, most likely because of the alumina skin on the top. A possible reason the gas injection experiments did not perform so well is the combination of the carbon which was present and the bubbles which agitated the surface. If this is the case then the exposed graphite plays a much larger part than the extra atmosphere entering the hood. Nevertheless both aspects should be improved upon for future experiments in this setup.

8.2 Remelting effect

The results obtained from both the remelting experiments, and the gas injection shows that most of the carbide can be removed just through holding the metal in a molten state. The same behaviour was seen in the results from the preliminary work, in addition to research performed by R. Dorward. [5] Comparing the results from the various experiments show two main trends:

- The carbide content is reduced with increasing holding time, shown in figure 35.
- The carbide content increased with increasing temperature shown in figure 36.

Dorward attributed the effect of remelting to poor wetting of carbide inclusions by the melt. [5] The small carbide inclusions move around in the molten aluminium until they collide with the crucible or the melt surface, once they do they are firmly attached and can be considered removed from the metal. Dorward also tried stirring the melt during the holding, and experienced even faster carbide removal, which is a strong indication that once a particle is removed through this mechanism it will not easily re-enter the melt as an inclusion. [5] Removal of inclusions through this mechanism would follow an expression such as the one shown in section 5.4, assuming that the rate of removal is proportional to the amount of inclusions remaining in the melt.

Carbide increasing with increasing temperature is also consistent with this mechanism of removal. Because removal to the crucible walls and the melt sur-

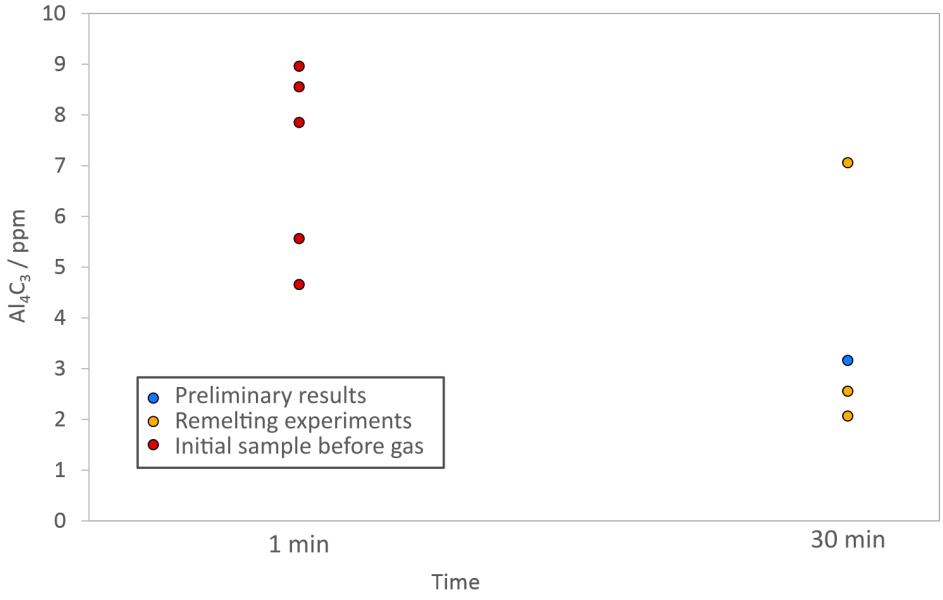

Figure 35: Remaining carbide after being remelted and held in a molten state for 1 min, and 30 min.

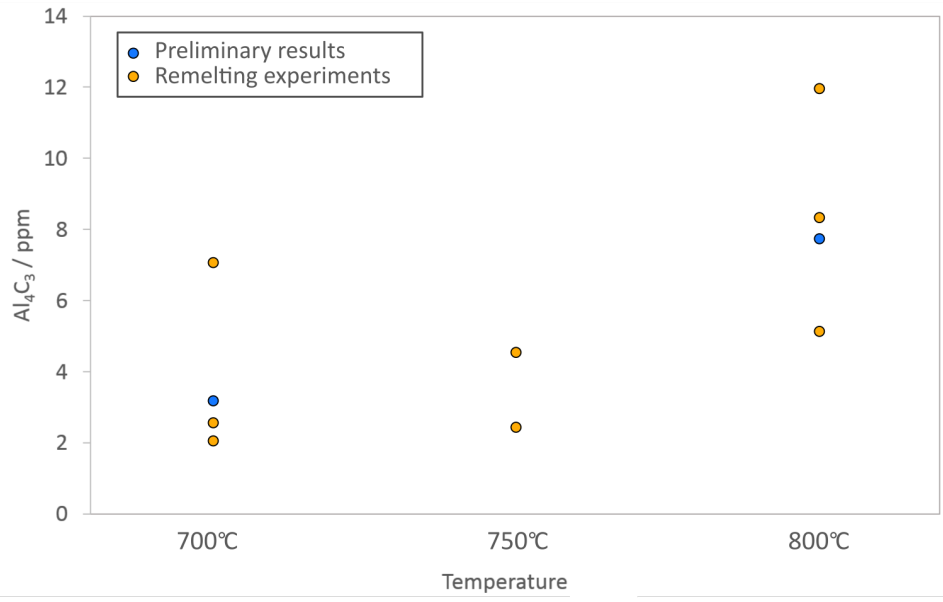

Figure 36: Remaining carbide after remelting at various temperatures.

face is only capable of removing solid inclusions, and not dissolved carbon, it is sensitive to temperature increases. By keeping the metal at a higher temperature the carbide inclusions dissolve into the melt. The dissolved carbon is unaffected by holding the metal in a molten state, so the inclusions are thus protected by the increased temperature. Because there is virtually no solubility of carbon in aluminium in its solid state the carbide inclusions will precipitate out when the temperature is reduced, or the metal is cast. [15] Figure 37 shows a simple drawing of how a higher temperature would effect this removal mechanism.

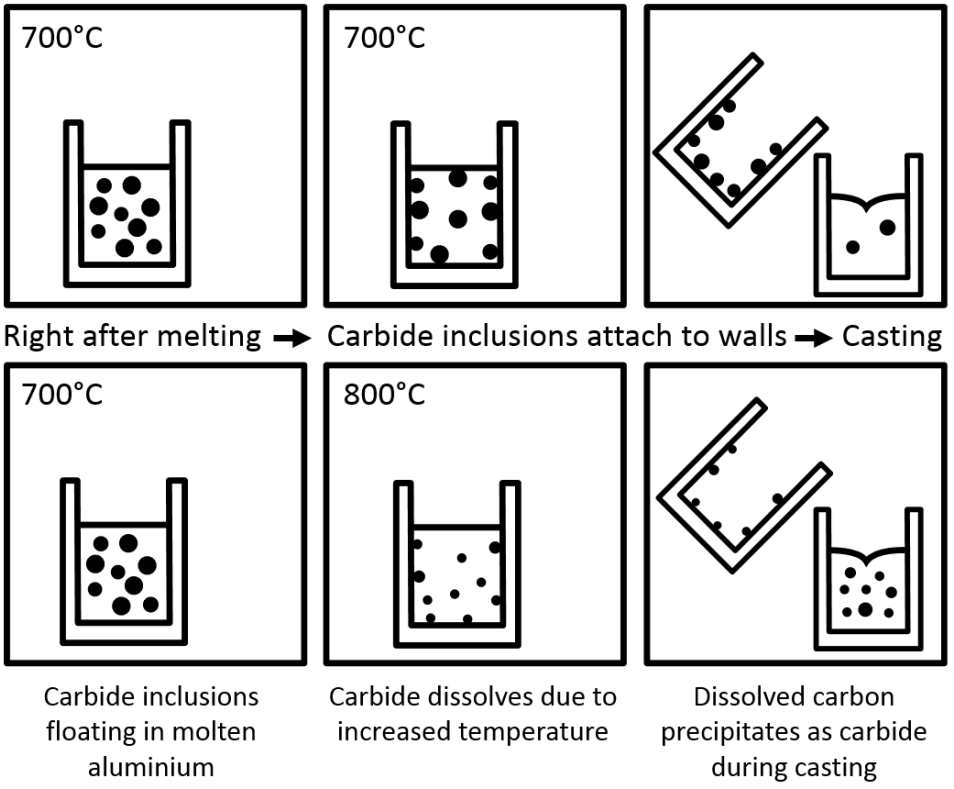

Figure 37: Effect of holding metal at an increased temperature.

8.3 Effect of H_2O

One of the key findings from the off-gas analysis taken during the gas injection experiments was that CH_4 formed when $H_2O(g)$ was blown through the melt. This is a strong indication that the water vapour is removing carbide from the melt through a chemical reaction.

Reaction 40 shows that a potential issue with adding H_2O to the melt is, that a reaction with the melt itself is also favoured thermodynamically, thus it is unlikely that the H_2O penetrates more than a short distance into the melt. [32] Thus it might be very difficult for a reaction between solid carbide and H_2O to take place.

$$\frac{2}{3}\,Al_4C_3(s) + H_2O\,(g) = \frac{1}{3}\,Al_2O_3(s) + H_2(g), \quad \Delta G_{T=700^\circ C} = -308.7kJ[3] \quad (40)$$

Due to the low amount of successful parallels it was not possible to see any clear difference in carbide removal when 1% H_2O was used compared to when 2% H_2O was used. Similarly no conclusive difference was seen in the size of methane peaks. If it is the case that 1% H_2O gives the same performance as when 2% is used that would be a very good result due to the safety risks of using water together with molten metal.

8.3.1 Possible chemical removal mechanisms

When considering the chemical reaction which removes the carbide there are, as mentioned in section 5.3.6, two possible reaction mechanisms.

- Removal of dissolved carbon, indirectly removing the carbide inclusions.
- Solid gas reaction, directly removing carbide inclusions.

The removal of dissolved carbon is the most simple one, removing the dissolved carbon changes the equilibrium between carbide and dissolved carbon which leads to the carbide dissolving back into the melt. On the bubble surface carbon reacts with the moist argon forming methane and CO within the bubble. A drawing displaying this removal mechanism is displayed in figure 38.

The other proposed mechanism is that H_2O introduced through the moist argon reacts directly with the carbide inclusions, as displayed in figure 39. This type of reaction mechanisms is described by the shrinking core model or topochemical model. [36]

$$\frac{1}{6}\,Al_4C_3(s) + H_2O\,(g) = \frac{1}{3}\,Al_2O_3(s) + \frac{1}{2}\,CH_4(g), \quad \Delta G_{T=700^\circ C} = -225.8kJ[3] \quad (41)$$

As time passes the alumina layer on the surface of the carbide inclusions grows thicker. After a while the removal rate of carbide is dependent on both the rate of the chemical reaction, and the rate of diffusion through the outer alumina layer.

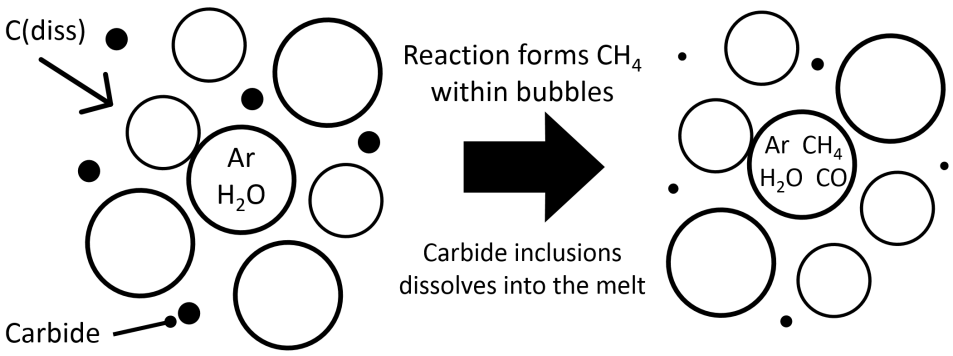

Figure 38: Dissolved carbon reacts with the moist argon being passed through the melt transforming it into methane, as the carbon content of the melt is reduced the carbide inclusions shrink because the equilibrium between carbon and carbide is shifted.

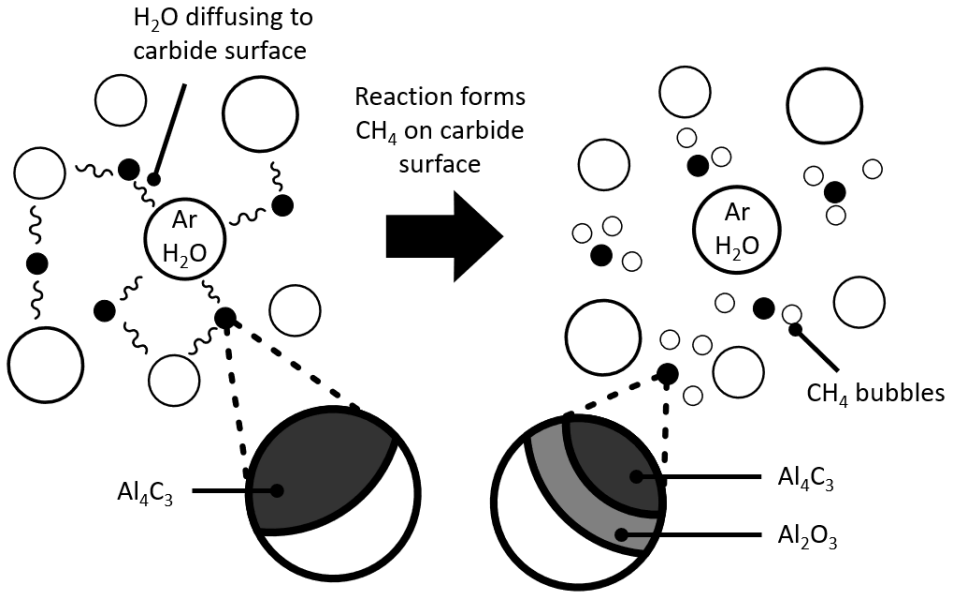

Figure 39: H_2O reacts at the carbide surface forming methane bubbles and alumina on the surface of the carbide inclusions.

It can be shown that in the case where the chemical reaction is rate determining, the time it takes to remove the carbide is proportional to the particle diameter, $t_{tot} \propto d_0$. While if the diffusion through the product layer is rate determining then the time it takes to fully react a carbide inclusion is proportional to the square of the diameter, $t_{tot} \propto d_0^2$. [36] The reaction for this mechanism is shown in reaction equation 41:

8.3.2 Discussion on which reaction mechanism occurs

A key feature of the solid-gas reaction is that no CO is expected to form according the reaction 41. This is not what was observed from the gas analysis obtained from the FTIR. The results instead point to the first removal mechanism being the most likely, reaction between dissolved carbon and H_2O. The main evidence is that there appears to be a correlation between the methane peak right after lance insertion and the CO. The chemical reaction for the removal mechanism is as follows: [3]

$$\frac{3}{2}\,\mathrm{C} + \mathrm{H_2O\,(g)} = \mathrm{CO\,(g)} + \frac{1}{2}\,\mathrm{CH_4(g)}, \quad \Delta G_{T=700^\circ C} = 4.412kJ[3] \tag{42}$$

One must also take into account that to keep the reaction going, carbide needs to dissolve, which increases the change in Gibb's energy. The complete reaction with ΔG is shown below:

$$\frac{3}{2}\,\mathrm{C} + \mathrm{H_2O\,(g)} = \mathrm{CO\,(g)} + \frac{1}{2}\,\mathrm{CH_4(g)}, \quad \Delta G_{T=700^\circ C} = 44.049kJ[3] \tag{43}$$

As methane is formed so will $\mathrm{CO\,(g)}$, so when a larger amount of methane forms a larger amount of CO is expected to form as well. The analysis of the off-gas from the experiments reveals this very behaviour. The experiments that had a large amount of methane forming had a very noticeable CO peak, while the experiments with a small amount of methane forming had no noticeable CO peak.

A third possible removal mechanism would be a mix of the two reaction mechanisms mentioned. The H_2O added to the melt reacts with both dissolved carbon and the solid aluminium carbide particles as in the following reaction:

$$\begin{aligned}\frac{3}{8}\,\mathrm{C} + \frac{1}{8}\,\mathrm{Al_4C_3(s)} + \mathrm{H_2O} = \frac{1}{2}\,\mathrm{CH_4(g)} + \frac{1}{8}\,\mathrm{CO\,(g)} + \frac{1}{4}\,\mathrm{Al_2O_3(s)},\\ \Delta G_{T=700^\circ C} = -214.633kJ[3]\end{aligned} \tag{44}$$

This reaction is much more strongly thermodynamically favoured than the the reaction with dissolved carbon, mostly due to the energy which is released by

aluminium reacting with the water present and forming Al_2O_3(s). On the other hand it is slightly less favoured thermodynamically than the solid-gas reaction, reaction 41, because some of the oxygen atoms in water would form CO instead of alumina, which releases much less energy.

A key aspect of reaction 43 and 44 is that they, to a lesser or greater degree, work on dissolved carbon. Because the solubility of carbon in molten aluminium is extremely low at low temperatures, increasing the temperature might help the removal by dissolving the carbide making much large amounts of carbon available to react. However, if the removal to walls as a result of wetting is a greater effect than the chemical removal reaction, then increasing the temperature would have deleterious effect on the carbide removal. Nevertheless, more measurements especially at a heightened temperature is needed to clarify this.

8.3.3 Methane formation

While the height of the methane peak was rather inconsistent across the various experiments that were performed, the same does not apply for the width, i.e the time at which methane formed. The duration in which methane formed only occurred for roughly 10 minutes, indicating that a much shorter gas injection time would be sufficient. This is also supported by the measurement performed 10 minutes after the gas injection begun, where a very low amount of only 1.8ppm carbide was detected.

For methane to form it needs a source of carbon. In the current experimental work there are four potential sources this carbon can come from:

- Dissolved carbon is a rather likely source because then a reaction may occur at the bubble surface as a result of the dissolved carbon diffusing to the bubble surface. As the reaction progresses the melt would be depleted of dissolved carbon unless it is replenished by carbide dissolving into the melt.

- Carbide particles floating in the bulk melt is another possible candidate, an issue with this source of carbon is that there is a rather sparse amount of particles present because some of the carbide particles will separate to the walls and surface, while some will dissolve in the melt.

- Carbide particles from the surface of the melt is another likely candidate, because the remelting effect causes the surface of the melt to get enriched with carbide. The carbide may also be firmly attached, [5] which would make it more difficult for it to move out of the way of bubbles. But once the

carbide is removed from the surface, the melt is mostly depleted of carbide which causes the reaction to stop.

- CO above the melt surface is also a possible carbon source. Due to the setup having exposed graphite parts, the atmosphere above the melt contains some CO. Reaction equation 45 shows how CO may react with water and form CO. While the reaction is favoured thermodynamically it usually requires a catalyst, a higher water content, and it is usually performed at lower temperatures where the ΔG of the reaction is much lower. [37, 38]

$$2\,\mathrm{CO\,(g)} + \mathrm{H_2O\,(g)} = \frac{1}{2}\,\mathrm{CH_4(g)} + \frac{1}{3}\,\mathrm{CO_2(g)}, \quad \Delta G_{T=700^\circ C} = -41.9kJ[3] \tag{45}$$

8.3.4 Estimation of carbide content during gas injection

It is possible to make a rough estimation of the carbide content of the melt during the early stage of the gas injection. Assuming that the rate of carbide removal is proportional to the rate of methane formation, the methane content of the off-gas may be integrated to obtain a curve which is proportional to the carbide content in the melt. The curve may be scaled so that the start-point and end-point matches the measured carbide content right after melting and after the gas-injection period. The mathematical approach is written below:

$$\frac{dc}{dt} \propto \frac{d[\%\mathrm{CH_4}]}{dt}$$

$$c(t) \propto \int_{t_0}^{t} \frac{d[\%\mathrm{CH_4}]}{dt} dt + c_0$$

The final expression, equation 46, is obtained through scaling such that the endpoint is c_1 which is the carbide measurement performed after the gas injection.

$$c(t) = c_0 + \left(\int_{t_0}^{t} \frac{d[\%\mathrm{CH_4}]}{dt} dt \right) \left(\frac{c_1 - c_0}{\int_{t_0}^{t_1} \frac{d[\%\mathrm{CH_4}]}{dt} dt} \right) \tag{46}$$

Figure 40 shows the result of using this expression on the data from the two experiments which had formation of both methane and CO. Those experiments are the only ones used because they had the strongest indication of a reaction. A weakness of this approach is that it only takes into account removal mechanisms which form methane, thus the remelting effect and reactions not forming methane are unaccounted for. Additionally the carbide measurement performed after the

gas injection is taken after 30 minutes while the methane formation is complete after just 10 minutes, which leads to additional uncertainty. Future experiments where a measurement is also performed immediately after the methane formation is completed, would eliminate this uncertainty.

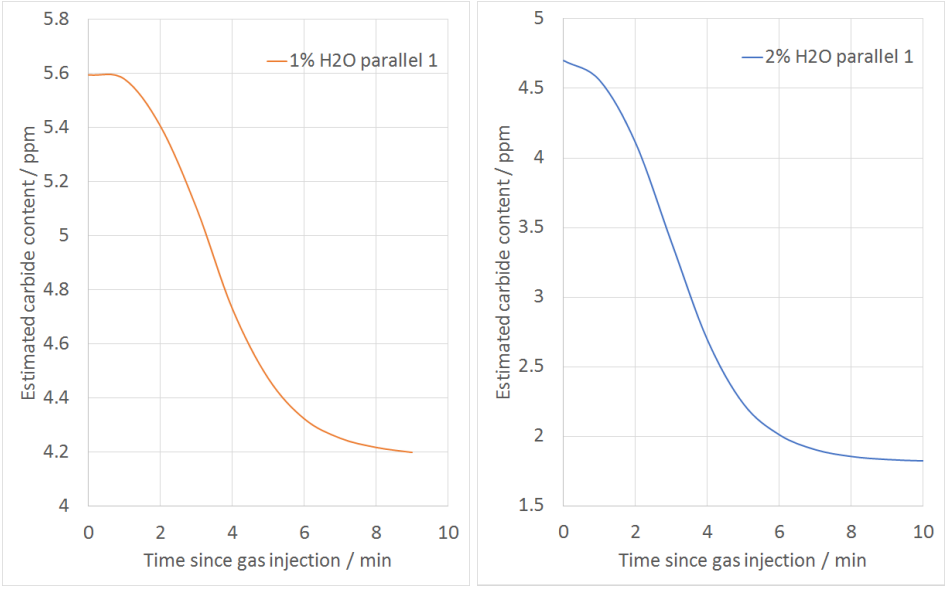

(a) 1% H_2O parallel 1.

(b) 2% H_2O parallel 1.

Figure 40: Estimated carbide removal during gas injection.

8.4 Carbide formation

After being held at 1100°C a fairly thick carbide layer formed at the surface contacting the graphite crucible, and a much thinner carbide layer formed at the rest of the surface. After the experiment the droplet was cooled from the outside, causing the surface layer to always be at a lower temperature than its interior. The lower surface temperature leads to a reduced carbon solubility in the surface layer of the particle, thus the surface has the greatest driving force for nucleation. Additionally the poor wetting of the aluminium on carbide means that there is a much lower driving force needed for heterogeneous nucleation on the surface than there is for homogeneous nucleation within the core of the droplet.

Below the surface large clusters of carbide particles could be found. Further away from the droplet surface there were not many particles. When viewing the sample in a microscope what is being viewed is just the a 2-dimensional cross

section of the sample, thus any 3-dimensional geometry of the particles can not be determined. One possible mechanism that would lead to the carbide clusters that was observed, is that the carbide grew as a network which originated from the surface of the droplet. It was attempted to scan the interior of the sample, but there was too poor contrast between the carbide clusters and aluminium.

SEM imaging revealed the carbide layer to be much thicker on the region of the droplet in direct contact with the graphite crucible. The thickness of the carbide layer surrounding region of the particle that was not in direct contact with carbon, was observed to be between a third and a sixth of the carbide layer in contact with the graphite crucible.

One possible explanation is that carbide formed at the graphite/droplet interface has contributions from both the carbon dissolved in the metal and from carbon or aluminium diffusing through the carbide layer forming additional carbide. [16] It is, however, unlikely that this carbide is due to aluminium diffusing into the graphite because the droplet was not firmly attached to the graphite crucible. Tilting the crucible slightly (less than 10°) caused the droplets to detach themselves.

Settling could also be a possible explanation. At melting temperature the density difference between the carbide and the metal is relatively low (2.375 g/cm^3 for Al and 2.36 g/cm^3 for Al_4C_3), but as the temperature increases the density of molten aluminium will decrease more than the density of carbide, because density of solids is more affected by temperature than liquids. It is still an open question if the density difference is enough to overcome the attachment force which keeps the carbide from entering the melt. If the attachment force is too great, then only carbide which formed homogeneously in the interior of the droplet may settle to the bottom.

9 Conclusions

- The experimental setup used for the gas injection experiments was able to produce results consistent with previous research. It could be improved if leaks through the edges and pouring spout on the furnace could be sealed better, and if the graphite parts could be avoided.
- The setup used during the remelting experiments performed similarly to the one used in the preliminary studies.
- Remelting the metal yielded a drastically reduced carbide content, as has been shown in previous studies, possibly due to wetting effects. [5, 1] Furthermore the dross samples were enriched in carbide giving additional support for this mechanism being the cause of removal.
- Increased temperature lead to less carbide being removed through the remelting effect. It may have been caused by the solubility of carbon in aluminium increasing with a higher temperature.
- Blowing argon with added water leads to methane forming which is a strong indication of the water removing the carbide from the molten metal. The CO content in the off-gas was positively correlated with the methane which indicates the reaction to be between dissolved carbon and water.
- Methane was only formed during the first 5-10 minutes of gas injection, meaning that 30 minutes gas injection time might be far more than required for decent carbide removal.
- From the current results it was not possible to see a significant difference in the final carbide content when comparing 1% H_2O to 2%.
- At 1100°C carbide could be formed in pure aluminium held in a graphite crucible. As the aluminium pellet cooled, carbide precipitated heterogeneously at the pellet surface. Interior of the pellet was mostly carbide free.
- Carbide also formed, but in much larger quantities, at the interface between the aluminium pellet and the graphite crucible. This is possibly due to a direct reaction between the graphite crucible and the aluminium pellet.
- The size of the carbide inclusions formed in the carbide formation experiments, and the carbide inclusions detected in the dross samples from the

preliminary studies and in the dross samples from the current gas injection experiments have a similar shape and size as has been reported previously.

10 Further Work

- Improve the setup for the gas injection experiments by reducing the amount of outside atmosphere that leaks into the hood, and reducing the amount of exposed graphite.
- Perform more parallels of the gas injection experiments to get a better impression of how changing the amount of H_2O that is injected into the melt affects its carbide content. If 1% has equal performance as 2%, finding the smallest required H_2O content before the removal becomes worse.
- Because the removal mechanism proposed acts on dissolved carbon, experiments at higher temperatures where the solubility of carbon is much higher should be performed.
- Remelting experiments should be performed in the setup used for the gas injection experiments, so a better idea of how much of the carbide removal can be attributed to remelting effect and how much can be attributed to chemical reaction can be determined. Remelting experiments must be performed at each temperature that gas injection experiments are performed at.
- To improve the accuracy of the carbide content estimation, experiments should be performed were carbide measurements are taken immediately after methane formation is finished. Improving the understanding of how fast the remelting effect is removing carbide would also improve the accuracy of the estimation.
- Perform experiments with varying bubble sizes, a simple first step would be to use a filter with a higher PPI than the one used for the current work.

References

[1] Trygve S. Aarnæs. Removal of aluminium carbide from liquid aluminium, January 2018.

[2] Christian Simensen. Gas-chromatographic analysis of carbides in aluminium and magnesium. *Fresenius' Zeitschrift für analytische Chemie*, 292(3):207–212, Jan 1978.

[3] Outotec. HSC 9 (software). 2017.

[4] Novák Bronislav. On the chemical and electrochemical formation of aluminium carbide in aluminium electrolysis, November 2013.

[5] R.C. Dorward. Aluminium carbide contamination of molten aluminium. *Aluminium*, 49(10):686–689, October 1973.

[6] Merete Tangstad. *Metal Production in Norway*. Akademika Publishing, 2013.

[7] P. Patel. On the effect of formulation and porosity on cathode performance, July 2009.

[8] *Introduction to aluminium electrolysis: Understanding the Hall-Héroult process*. Aluminium-Verlag, Düsseldorf, 2nd ed. edition, 1993.

[9] Abdelhalim Zoukel, Patrice Chartrand, and Gervais Soucy. Study of aluminum carbide formation in hall-heroult electrolytic cells. *Light Metals 2009*, pages 1123–1128, 2009.

[10] P. Waite. A technical perspective on molten aluminum processing. In *Essential Readings in Light Metals*, volume 3, pages 51–58. John Wiley and Sons, April 2013.

[11] Paul K. Trojan and Richard Fruehan. Inclusion-forming reactions. In *ASM Handbook, Volume 15 - Casting*, pages 74–83. ASM International, 2008.

[12] Lucas Nana Wiredu Damoah and Lifeng Zhang. Removal of inclusions from aluminum through filtration. *Metallurgical and Materials Transactions B*, 41(4):886–907, Aug 2010.

[13] Christian Simensen. Comments on the solubility of carbon in molten aluminium. *Metallurgical Transactions*, 20A:191, 1989.

[14] R. Dorward. Discussion of "comments on the solubility of carbon in molten aluminum". *Metallurgical Transactions A*, 21(1):255–257, January 1990.

[15] J. Rødseth, B. Rasch, O. Lund, and J. Thonstad. Solubility of carbon in aluminium and its effect upon the casting process. *Light Metals*, pages 883–888, 2002.

[16] T. Etter, P. Schulz, M. Weber, J. Metz, M. Wimmler, J.F. Löffler, and P.J. Uggowitzer. Aluminium carbide formation in interpenetrating graphite/aluminium composites. *Materials Science & Engineering A*, 448(1):1–6, 2007.

[17] P. Patel, M. Hyland, and F. Hiltmann. Influence of internal cathode structure on behavior during electrolysis part ii: Porosity and wear mechanisms in graphitized cathode materials. 4:1017–1022, April 2013.

[18] B. Novak, K. Tschöpe, A.P. Ratvik, and T. Grande. *Fundamentals of Aluminum Carbide Formation*, pages 1343–1348. John Wiley & Sons, Inc., 2012.

[19] Sarina Bao, Kai Tang, Anne Kvithyld, Thorvald Abel Engh, and Merete Tangstad. *Wettability of Aluminium with Aluminium Carbide (Graphite) in Aluminium Filtration*, pages 1057–1062. John Wiley & Sons, Inc., 2012.

[20] R.C. Dorward. Reaction between aluminum and graphite in the presence of cryolite. *Metallurgical Transactions*, 4(1):386–388, January 1973.

[21] B. Novak, K. Tschöpe, A.P. Ratvik, and T. Grande. The effect of cryolite on the formation of aluminum carbide at the carbon aluminum interface. pages 1245–1250, 2013.

[22] Rolf Ødegård. On the solubility and electrochemical behaviour of aluminium and aluminium carbide in cryolitic melts, 1986.

[23] T. Engh. *Principles of Metal Refining.* Oxford Science Publications, 1992.

[24] M. Maniruzzaman and M. Makhlouf. Mathematical modeling and computer simulation of the rotating impeller particle flotation process: Part ii. particle agglomeration and flotation. *Metallurgical and Materials Transactions B*, 33(2):305–314, April 2002.

[25] U. Lindborg and K. Torsell. A collision model for the growth and separation of deoxidation products. *Trans. AIME*, 242:94–102, 1968.

[26] Andrew Szekely. The removal of solid particles from molten aluminum in the spinning nozzle inert flotation process. *Metallurgical Transactions B*, 7(2):259–270, June 1976.

[27] Neil J. Keegan and Steve F. Ray. An evaluation of industrial filtration systems. (casthouse). *Aluminium International Today*, 15(2), March 2003.

[28] D.V. Neff and Robert P. Pischel. Molten-metal filtration. pages 1–1, 2008.

[29] M. Maniruzzaman and M. Makhlouf. Mathematical modeling and computer simulation of the rotating impeller particle flotation process: Part i. fluid flow. *Metallurgical and Materials Transactions B*, 33(2):297–303, April 2002.

[30] Sarina Bao. Filtration of aluminium-experiments, wetting,and modelling, January 2012.

[31] Yu. V. Naidich, Yu. N. Chubashov, N. F. Ishchuk, and V. P. Krasovskii. Wetting of some nonmetallic materials by aluminum. *Soviet Powder Metallurgy and Metal Ceramics*, 22(6):481–483, Jun 1983.

[32] D.A Porter and K.E Easterling. *Phase Transformations in Metals and Alloys.* Chapman and Hall, 1991.

[33] G. K Sigworth and T. Engh. Refining of liquid aluminium : a review of important chemical factors, 1982.

[34] N. Eustathopoulos, J. Joud, P. Desre, and J. Hicter. The wetting of carbon by aluminium and aluminium alloys. *Journal of Materials Science*, 9(8):1233–1242, August 1974.

[35] Fourier transform infrared spectroscopy (ftir) : methods, analysis, and research insights, 2017.

[36] Terkel Rosenqvist. *Principles of extractive metallurgy.* Tapir Academic Press, Trondheim, 2nd ed. edition, 2004.

[37] Takafumi Sato, Takeyuki Suzuki, Mitsuhiro Aketa, Yasuyoshi Ishiyama, Kenichi Mimura, and Naotsugu Itoh. Steam reforming of biogas mixtures with a palladium membrane reactor system. *Chemical Engineering Science*, 65(1):451–457, 2010.

[38] P. Kowalik, K. Antoniak-Jurak, M. Błesznowski, M.C. Herrera, M.A. Larrubia, L.J. Alemany, and I.S. Pieta. Biofuel steam reforming catalyst for fuel cell application. *Catalysis Today*, 254(C):129–134, October 2015.